THESIS FOR THE DEGREE OF LICENTIATE OF ENGINEERING

Conjugated polymers on plasmonic metasurfaces for high contrast electronic paper in color

OLIVER OLSSON

Department of Chemistry and Chemical Engineering

CHALMERS UNIVERSITY OF TECHNOLOGY

Gothenburg, Sweden 2021

Conjugated polymers on plasmonic metasurfaces for high contrast electronic paper in color

OLIVER OLSSON

Technical report no 2021:19

Department of Chemistry and Chemical Engineering

Chalmers University of Technology

SE-412 96 Gothenburg

Sweden

Telephone + 46 (0)31-772 1000

Cover Image: Red, green and blue plasmonic metasurfaces in a stripe shape with PProDOT-Me_2 polymerized on the green area. To the left PProDOT-Me_2 is in the absorbing state while in the right is it in bleached state

Printed by Chalmers Reproservice

Gothenburg, Sweden, 2021

Conjugated polymers on plasmonic metasurfaces for high contrast electronic paper in color

Oliver Olsson
Department of Chemistry and Chemical Engineering
Chalmers University of Technology

Abstract

Electronic paper is the collective name of displays that, instead of emitting light, reflect the ambient light. These displays are known to have good readability in daylight and very low power consumption. However, there is a lack of electronic paper in color with high contrast and the ability to achieve video speed. This work presents that by utilizing a plasmonic metasurface, highly reflective subpixels in red, green, and blue can be achieved. Electrochromic materials are used to modulate the reflectivity, turning the pixels ON and OFF.

Conjugated polymers, such as polypyrrole, polyethylenedioxythiopene (PEDOT), and poly(dimethyl-propylenedioxythiophene) (PProDOT-Me_2), are known for their electrochromic properties and are evaluated for their optical performance in organic solvent on a thin gold film. The optical contrast of a film depends on both the polymer and the thickness, and it is found that by measuring the optical extinction in both the bleached (transmissive) state and the colored (absorbing) state of an arbitrary thickness, the maximum contrast of the polymer can be extracted by using the ratio of the optical extinction values.

PProDOT-Me_2 is shown to have the highest maximum contrast and is electropolymerized on top of the red, green, and blue plasmonic metasurfaces with an excellent optical contrast of 50%-60%. Tungsten oxide is evaluated as an inorganic electrochromic option and compared with PProDOT-Me_2—Its optical contrast is around 60% for all samples. The bistability is in favor of tungsten oxide, which showed little to no change after 1000 s, while PProDOT-Me_2 has a slight change after 100 s. On the contrary, PProDOT-Me_2 had a switching time of less than two seconds, while tungsten oxide had ten times higher.

For PProDOT-Me_2, the distance between the electrodes with the polymer and the counter electrode influences the switching time. Reducing this distance below 1 mm and using a suitable solvent resulted in a time between 10-50 ms, i.e. in the video speed regime. By producing a positive curvature on the electrode and deposit the polymer, it is also possible to keep the contrast high with video speed.

Using fast pulses also facilitated to switch the polymer from bleached to colored more than 10 million times with low degradation using an ionic liquid. The previously reported number of switches is one order of magnitude less.

Keywords: reflective display, conjugated polymers, PProDOT-Me_2, plasmonic electronic paper, electrochromism

List of publications

I. **Video Speed Switching of Plasmonic Structural Colors with High Contrast and Superior Lifetime**
Kunli Xiong, Oliver Olsson, Justas Svirelis, Chonnipa Palasingh, Jeremy Baumberg and Andreas Dahlin
Adv. Mater. **2021**, 2103217

II. **High-contrast switching of plasmonic structural colors: inorganic versus organic electrochromism.**
Marika Gugole*, Oliver Olsson*, Kunli Xiong, Jolie C. Blake, José Montero Amenedo, Ilknur Bayrak Pehlivan, Gunnar A. Niklasson, and Andreas Dahlin
ACS Photonics **2020** *7,* 7, 1762-1772
*Contributed equally as first authors

III. **Switchable Plasmonic Metasurfaces with High Chromaticity Containing Only Abundant Metals**
Kunli Xiong, Daniel Tordera, Gustav Emilsson, Oliver Olsson, Ulrika Linderhed, Magnus P. Jonsson, and Andreas B. Dahlin
Nano Lett. **2017**, 17, 11, 7033–7039

Contribution to the listed publications

I. Co-author. Developed methodology for polymer deposition and analysis.

II. Shared first author. Developed methodology for deposition and analysis of organic materials. Conducted all experiment of the organic materials.

III. Co-author. Fabricated electrochromic devices within the project. Similar devices were used in the publication.

Contents

1 Introduction

Displays are one of the most used human-to-computer interfaces. The most common use today is smartphones and computer monitors, which utilize a liquid crystal display (LCD) or organic light-emitting display (OLED) technology [1]. Recently there has been an increasing interest in reflective displays, also known as electronic paper, which instead of producing its own light, reflects the light from the environment, exactly like a book or a newspaper.

Various technologies have been utilized to create electronic paper. One of the earliest was the reflective LCD which is common in calculators and electronic shelf labels. The most successful technology was introduced in the late '90s and is called the electrophoretic display (EPD). It consists of microcapsules with charged black and white pigments. The pigments are transferred within the microcapsule by an applied voltage and thus change the color for the viewer, a schematic is seen in Figure 1. EPD is the technology behind E-Ink and is commercially available in e-readers such as the Amazon Kindle [2].

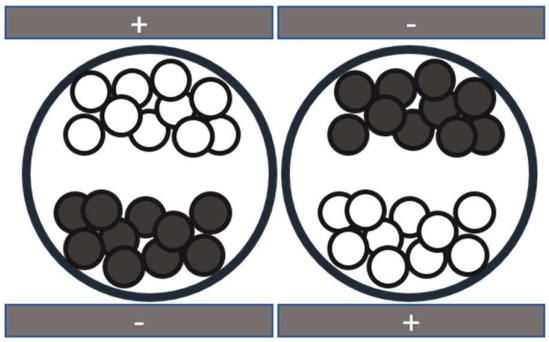

Figure 1 The EPD is moving charged particles up and down inside microcapsules. Thus changing the color from black to white.

Electrowetting is another technique that utilizes small confined capsules where a colored oil is moved in and out of visibility to tune the pixel's reflection [2]. In contrast to EPD, this technique has shown to have video speed [3], however, there is still no commercial product on the market.

Compared with an ordinary newspaper that has 60% reflection at the non-printed part and ~10% at the printed parts, the EPDs can achieve 40% to 4% while the reflective LCD technology can reflect between 33% and 5% [4]. In color, the reflection for EPDs becomes low with around 10-15% for each color, red, green and blue [5]. Thus, there is a need to find other techniques which have a higher reflection.

One of the key advantages of electronic paper is that its power consumption is very low since it does not emit light [4]. Another factor is the readability in daylight. To be able to see an ordinary emissive screen, the emission must be more intense than the light of the reflected ambient light. As with ordinary paper, this is not a problem for e-paper [6].

Recently, there has been an interest in using nanostructures to create electronic paper in color. Incident light undergoes constructive and destructive interference when interacting with a certain structure and the reflected light can be colored. This is called structural coloring. If the structure contains metal the light could couple to the electrons and create a plasmonic effect which also can result in coloring [7, 8]. Different approaches such as combining anisotropic plasmonic metasurface with liquid crystals to alter the polarization and change the reflection have been made [9]. Another approach is to create a plasmonic metasurface with high reflection and utilize electrochromic materials to alter it [10]. The latter is used in this work.

2 Theory

2.1 Structural colors and plasmonic color generation

Nature is frequently using structural colors. Many animals, such as butterflies and birds, generate their colors by having a submicrometer periodic structure of their feathers. Different from a standard pigment, which absorbs light on a molecular scale, the difference in refractive index generates the color. Reflection occurs wherever there is a mismatch in the refractive index, and summing up all the reflection, constructive or destructive interference occurs [11].

While nature has used dielectrics to create structural colors, man has used metals to generate plasmonic color generation for thousands of years, and early uses were the colored church windows which contain gold nanoparticles. Over the past years, more focus has been drawn to plasmonic color generation because of its easy manufacturability and ease of recyclability since most materials have the same element but different geometry [12].

In materials with loosely bound electrons, such as metals, a cloud of free electrons is present which can start oscillating when excited. The quantized electron oscillation of the free electron cloud is called a plasmon, or a bulk plasmon. In certain conditions, light couples to plasmons on the boundary between a metal and a dielectric. The light will then be absorbed and transform into a *surface plasmon polariton* (SPP) which propagates on the boundary [13].

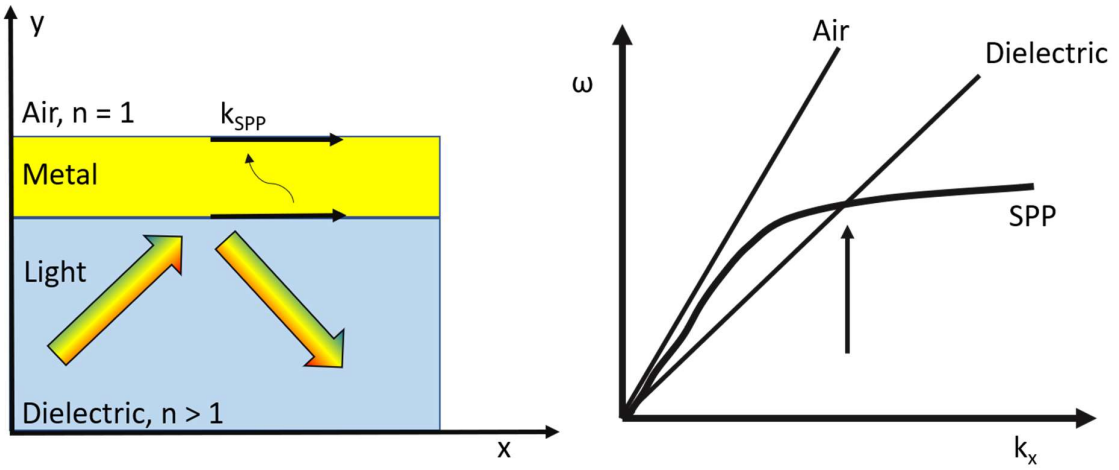

Figure 2 To the left: A surface plasmon polariton is excited on the air-metal boundary by the incident light on the metal-dielectric side. To the right: The dispersion relation of surface plasmon polaritons (SPPs). The momentum of the incident light in the air never matches the momentum of the SPP. A dielectric is used to increase the momentum to match the energy, indicated by the arrow.

By solving Maxwell's equations, a dispersion relation for the surface plasmon polariton is obtained. When the photon momentum, k_x, and energy, ω, match, the plasmon can be excited. For light propagating in air, the momentum is too low to match the dispersion for SPP. A material with a higher refractive index, such as glass, is used to increase the momentum. A schematic of the dispersion relation is shown to the right in Figure 2 where the arrow indicates the possible momentum and energy where an SPP can be excited.

The x-component of the incoming light is required to have a nonzero value so for a planar surface to excite SPPs, the incident light is radiated at a high angle. A schematic of the process can be seen to

the left in Figure 2 where light in a dielectric is radiated onto a metal surface with an angle. The SPP is propagating on the air-metal boundary in x-direction and decaying in y-direction [13].

Another way of exciting plasmons is to use a grating that will phase match the incident light to the SPP [13]. If the metal has a periodic or quasiperiodic structure, it will act as a grating; diffracted light will couple with the electron cloud in the metal and excite SPPs. The light is absorbed and can be scattered. For nanohole arrays, a spectral feature that behaves like a localized resonance will also occur at slightly greater wavelengths than the absorption, generating an transmission minimum [14].

The dispersion relations for the electromagnetic field throughout a metal-insulator-metal (MIM) structure can be found by solving the boundary value problem of Maxwells' equations. The wavelength of the optical extinction peak can be found where it matches the wavelength of one of the SPP-mode excited by the periodic hole array [15, 16].

A colored pixel can be fabricated by a MIM-structure consisting of; a silver layer as a back reflector, an insulating layer consisting of aluminum oxide, and a top reflector of 20 nm gold film creates a Fabry Perot cavity, which generates absorption in the reflection spectrum. However, the absorption occurs at a too narrow wavelength interval to create the green and blue pixels solely, and too much red light will be reflected [10].

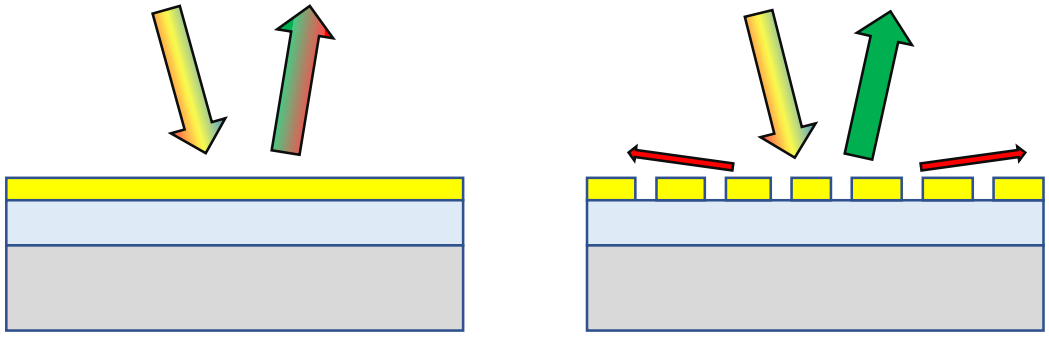

Figure 3 To the left: Schematic of the structure which generates a color by structural coloring. To the right: Enhanced coloration due to plasmonics.

By introducing nanoholes in the top gold reflector surface plasmons can be excited and scatter the red light, thus enhancing the coloration [10]. A schematic can be seen in Figure 3 where a green pixel is desired. To the left, without holes and plasmonic effect, red color is included. To the right, the red light is scattered, due to the plasmonic effect introduced by a nanohole array, leaving a pure green color. The plasmonic effect is dependent on both the size of the holes and the distance between them, where it has been shown that a larger distance between the holes scatters light of longer wavelengths [17].

2.2 Electrochemistry

Generally, but not exclusively, electrochemistry is the branch in chemistry that studies the electron transfer between a solid conductive material and a solution. The solid material is usually a metal such as platinum or gold. The solution is most commonly a solvent with an analyte, the compound which is analyzed. Additional salt is usually dissolved in the solvent to increase the conductivity. Salt dissolved in a solvent is an electrolyte and common examples are sodium chloride in water, or lithium perchlorate in propylene carbonate. The latter is frequently used in this thesis.

The analyte can be reduced, gaining an electron, and/or oxidized, losing an electron (Equation 1). Both these reactions where there is an electron transfer between solution and the metal, are called *Faradic*. The concentration of the reduced species and the oxidized species on the surface of the metal depends on the applied potential to the metal. The relation between the concentrations and the potential is formulated in *The Nernst equation* (Equation 2). The potential, E, is relative to the species *formal potential*, $E^{0'}$, the potential measured against a *standard hydrogen electrode* when the concentration of the reduced species, C_{red}, is equal to the concentration of the oxidized, C_{ox}. The remaining constants are; F – faradays constant, R – the gas constant, T – the temperature in Kelvin, n – number of electrons transferred, often n=1 [18].

$$O+ne^- \rightleftarrows R \tag{1}$$

$$E-E^{0'}=\frac{RT}{nF}\ln\frac{[C_{ox}]}{[C_{red}]} \tag{2}$$

In the bulk, the concentration follows the *Nernst-Planck equation* (Equation 3). The temporal concentration difference is equal to 3 terms. The first terms are *diffusion* where D is the diffusion constant. The second term is a *convection* term where u is the velocity. The third term is *migration*, drift in an electric field where z is the charge of the species, +1, +2 etc. $\nabla\varphi$ is the potential gradient in absence of magnetic fluxes [18].

$$\frac{\partial c}{\partial t}=\nabla\left[D\nabla c-uc+D\frac{Fz}{RT}c\,\nabla\varphi\right] \tag{3}$$

In the case of no convection and no migration, the equation reduces to Equation 4, which is Fick's second law. The molar flux, J, is the number of species transported per time and area, A. If diffusion is limiting the reaction at electrode surface, Fick's first law (Equation 5) describes the number of reduction/oxidation events at the surface. The electric current is related to the flux by Equation 6 where n is, again, the number of charges transferred per molecule, F – faradays constant, and A – area [18].

$$\frac{\partial c}{\partial t}=D\frac{\partial^2 c}{\partial x^2} \tag{4}$$

$$J=-D\frac{\partial c}{\partial x} \tag{5}$$

$$I=-n\,F\,A\,J_{Ox}(x=0) \qquad 6$$

If the bulk is consisting of a species in the oxidized state and reduction potential is applied to the electrode, the boundary concentration will alter according to the Nernst equation. However, given that the reaction happens instantly when a molecule reaches the surface, the current will depend only on the diffusion of oxidized species into the electrode. The relationship of current and time is summarized in *the Cottrell equation* (Equation 7) where c_0 is the bulk concentration. The Cottrell equation is obtained by solving Fick's second law (Equation 4) together with Fick's first law (Equation 5) as boundary condition. Experiments, when current is measured with constant applied potential, is called chronoamperometry [18].

$$I=\frac{nFAc_0\sqrt{D}}{\sqrt{\pi t}} \qquad 7$$

Cyclic voltammetry (CV) is a common experiment where the potential is swept over a potential range with a fixed rate in a triangular wave and the current is measured and plotted against the potential. A simulation [19] can be seen in Figure 4 where a concentration of 1 mM and a diffusion constant of 10^{-5} cm^2/s was used. The scan rate was 100 mV/s.

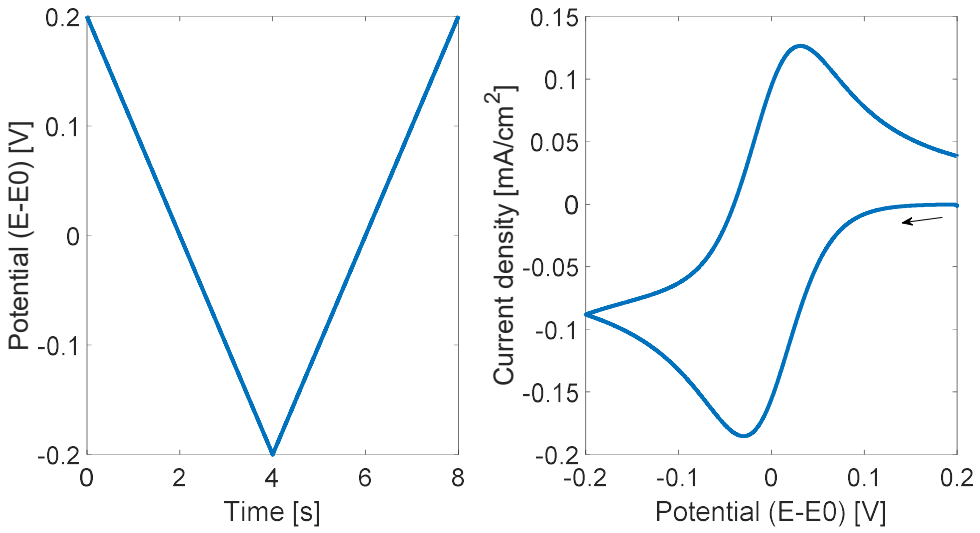

Figure 4 To the left: The potential over time. To the right: Simulated current response plotted against the potential generating a CV-diagram. The simulation uses a concentration of 1 mM and a diffusion constant of 10^{-5} cm^2/s.

The current peaks in the CV diagram indicates at which potential the diffusion towards and from the electrode occurs the fastest. The reduction peak potential, negative, and the oxidation peak potential, positive, is separated due to this diffusion. The value of the peak current is proportional to the concentration, diffusion constant, and the square root of the scan rate. This relationship is summarized in *the Randle-Sevcik equation* (Equation 8). The scan rate dependence of the CV diagram is shown in Figure 5 [18].

$$I_p = 0.4463\, nFAc_0 \sqrt{\frac{nFDv}{RT}} \qquad 8$$

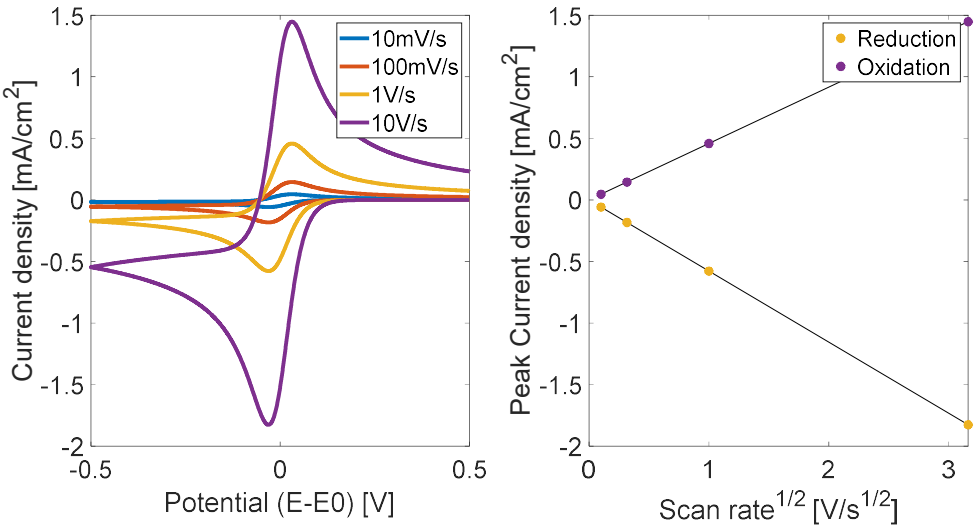

Figure 5 To the left: Simulations of CV diagrams for various scan rates. The concentration is 1 mM and the diffusion constant is 10^{-5} cm^2/s. To the right: The peak currents plotted against the square root of the scan rate displays a linear relationship.

Nernst equation assumes that the electron transfer on the electrode boundary is fast (the species are in equilibrium for the given potential) which is not always the case. By introducing another regulating term on the boundary, the slow, or *sluggish kinetics,* can be addressed with two new parameters: k_0, the standard rate constant, and α, the symmetry factor. Equation 9 states the current where the kinetic parameters k_f and k_b are defined in Equation 10 and 11. The subscripts 'f' and 'b' are forward and backward respectively where forward is left to right in Equation 1 and backward is left to right [18].

$$I = nFA\,[C_{red}(x=0)\, k_b - C_{ox}(x=0)\, k_f] \qquad 9$$

$$k_f = k_0 e^{-\alpha \frac{nF}{RT}(E-E_0)} \qquad 10$$

$$k_b = k_0 e^{(1-\alpha) \frac{nF}{RT}(E-E_0)} \qquad 11$$

With more sluggish kinetics (lower k_0) the peaks in the CV diagram separates further. The symmetry factor, α, is a measure of in which direction the reaction is 'favored' and is for most reactions 0.5 (no preference) but it is not uncommon that it can be between 0.2 and 0.8 (Figure 6) [18].

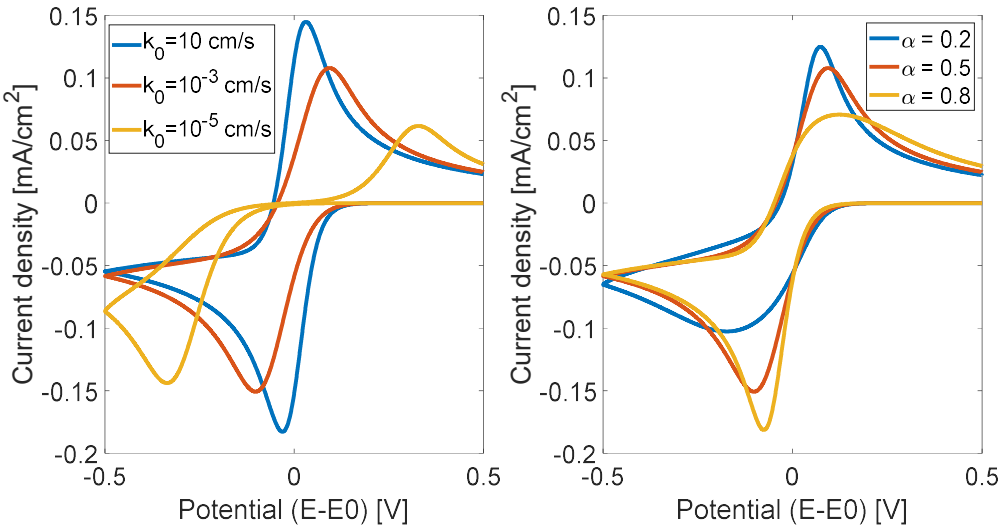

Figure 6 To the left: Peak separation can be seen when the standard rate constant decreases. To the right: How the symmetry factor alters the CV diagram.

In the case where the analyte is adsorbed on the surface, no diffusion takes place, and the equations get reduced to only the boundary (Equation 12 and 13) [20, 21].

$$\frac{d\Gamma_{ox}}{dt} = -k_f\Gamma_{ox} + k_b\Gamma_{red} \qquad 12$$

$$\frac{d\Gamma_{red}}{dt} = +k_f\Gamma_{ox} - k_b\Gamma_{red} \qquad 13$$

Here Γ_{ox} and Γ_{red} are the surface concentrations and k_f and k_b, are the previously introduced kinetic parameters (Equation 10 and 11). Solving the system of equations for a fast (not sluggish), symmetrical (α= 0.5) reaction with a maximum surface concentration of 10^{-9} mol/cm^2 and different scan rates generates CV diagrams which can be seen in Figure 7.

There is no peak potential separation when α=0.5 but in the case where α is different from 0.5, some peak separation occurs (not shown). The difference between the freely diffusive species and the adsorbed species is that the current declines to zero after the peaks because there are no more species to oxidize/reduce and that the peak current *is linear* with the scan rate [18].

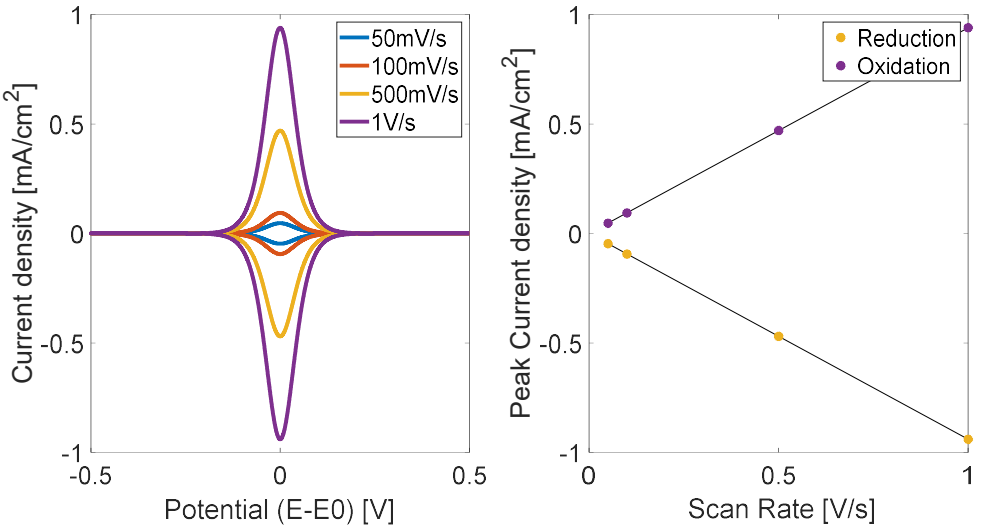

Figure 7 To the right: A CV diagram of a surface adsorbed species with different scan rates. To the right: The peak current can be seen to vary linearly with the scan rate.

When a potential is applied to the electrode there will also be a *double-layer* of ions that builds up on the surface. An analogy is an electrical capacitor that can be charged and discharged. The amount of charge the electrical capacitor stores is linear with the applied voltage and how much charge a capacitor can store depends on its capacitance, Equation 14 and 15 [18].

Assuming that the charging of the double layer is an electrical network with a capacitor with a capacitance C in series with a resistor with the value R, the current for a static potential step falls exponentially and is described by Equation 16. The CV diagram will have a box-like look where the plateau current will be linear with the scan rate and the capacitance, Figure 8. The current measured is called *capacitive currents* and is a part of *non-Faradic currents* [18].

$$C=\frac{q}{V} \tag{14}$$

$$I(t)=C\frac{dV(t)}{dt} \tag{15}$$

$$I(t)=\frac{V}{R}e^{-t/RC} \tag{16}$$

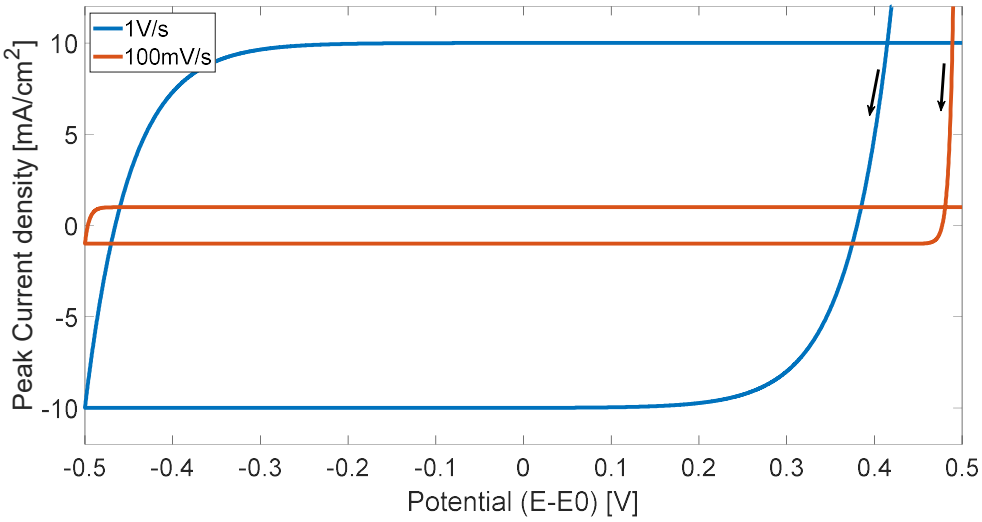

Figure 8 A simulation of a potential sweep for a network of a resistor (5 Ω) and a capacitor (0.01 F) in series displays a 'box-like' s.

2.3 Electrochromic conjugated polymer

Electrochromism is the property of a material to change its color with an applied voltage. The material is either dissolved in an electrolyte or coated on an electrode that is immersed in an electrolyte. Upon electrochemical oxidization and reduction, the material changes its bandgap and alters the absorption, leading to a change in color. Applications include eyewear, smart-windows, camouflage materials, and electronic shelf labels. The most famous materials which exhibit these properties are metal oxides, viologens, conjugated polymers, and Prussian Blue [22, 23]. Focused in this work, are the class called conjugated polymers which are briefly compared with the inorganic tungsten trioxide. Conjugated polymers are a class of polymers that have an alternating single and double bond between carbon atoms, thus producing delocalized electrons or a conjugation.

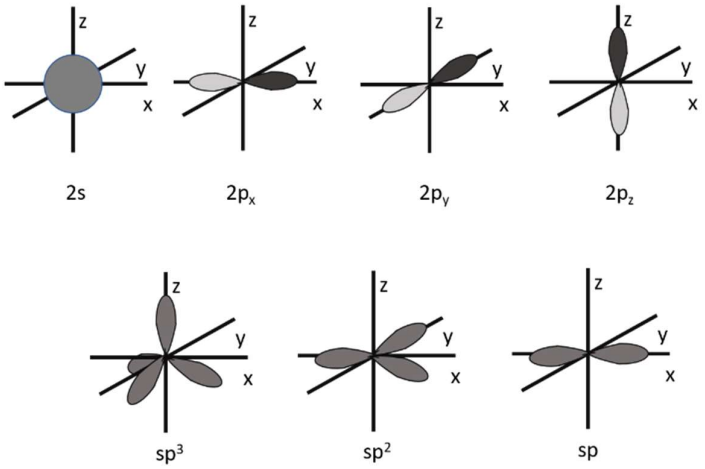

Figure 9 Top row: Orbitals of the valence electrons of carbon from the symmetric 2s to the three variations of the 2p-orbitals. The different shading of the 2p-orbitals represents the sign of the orbitals wavefunction. The bottom row: The three different hybridizations going from sp^3 to sp^2 and finally sp.

Quantum mechanics tells us that an electron is not in one place but smeared out in space and is described by a wave function. *Atomic orbitals* are used to describe how the electron's wave function looks like in an atom. Carbon has six electrons, where two electrons are in the bound 1s-orbital and two electrons are in the 2s-orbitals. The remaining two electrons are in the $2p_{x,y,z}$-orbitals. The 2s-orbital can be mixed with the 2p-orbital. This is called *hybridization* and three different mixed states are available, sp, sp^2, and sp^3, where the superscript indicates how many p-orbitals are included in the mixed state. Figure 9 displays the atomic orbitals for the 2s and the 2p -orbitals and the three hybridizations.

When two atoms are bonded together the *molecular orbitals* are formed. In the case of two carbon atoms bonded together where both are hybridized in sp^2-orbitals two bonds will form. One bond is made by overlapping orbitals, a σ-bond, Figure 10 to the left. The remaining p-orbitals will bond together and form a π-bond. The molecular orbitals are split into *bonding,* σ and π, and *anti-bonding*, σ* and π*, where electrons are located into the *bonding* orbitals with lower energy. The highest energy level which is occupied with electrons is called HOMO, *highest occupied molecular orbital.* The lowest energy which is unoccupied is called LUMO, *lowest unoccupied molecular orbital* [24-26].

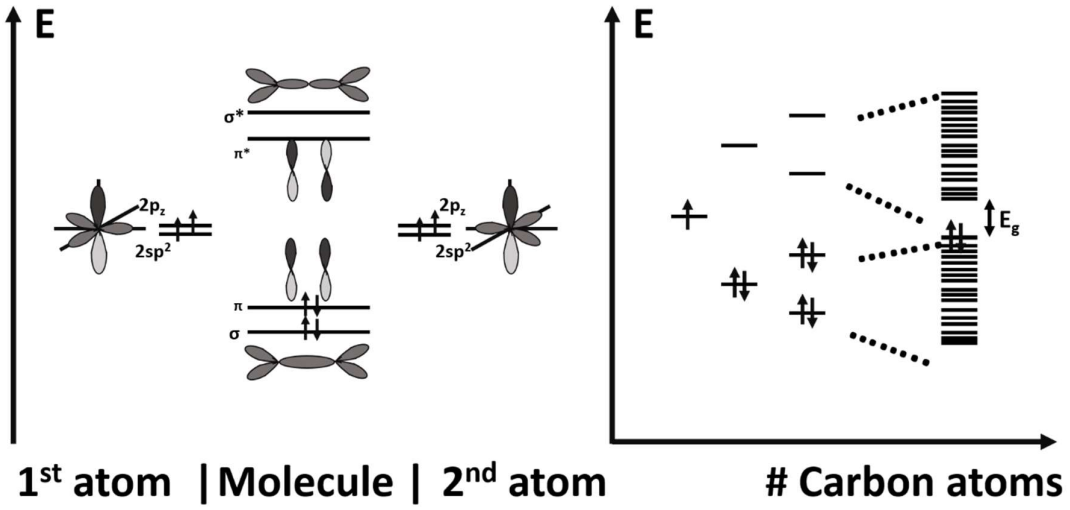

Figure 10 To the left: A molecular orbital forms from two atomic orbitals. The two atomic orbitals have one sp2 hybridization each which forms the bonding σ-bond with lower energy and the antibonding σ-bond with higher energy. The π-bond is formed by the $2p_z$-orbitals are, as the σ-bond, split into bonding and antibonding. To the right: Formation of the electronic-bands with increasing amount of carbon atoms each contributing with one electron in the $2p_z$-orbital.

When carbon atoms are added into a chain there will be an alternation between a double bond (one σ -bond and one π-bond) and a single bond (one σ -bond). The energy levels will further split and eventually merge into bands with an energy gap. The lower energy band is called *valence band* and are occupied with electrons, HOMO is now the valence band edge. Figure 10, to the right, displays the evolution of the energy states when carbon atoms are added, only the electrons in the 2p-orbital is shown. The higher energy band is called *conduction band* and is vacant thus making its bands edge LUMO. There is a gap because the conjugation length is finite and also because of *Peierl's distortion*, or transition, which says that the spacing between the atoms in a one-dimensional crystal is not uniform but has two different values [25-27].

In the conjugated polymers there is an alternation of the single and double bond which makes one bond longer than the other [25]. The energy gap, or bandgap, makes the polymer a semiconductor instead of a metal [27] and is also what gives rise to the colors in conjugated polymers by absorption of equal energy light [26]. However, in a film of conjugated polymers, there is also an interaction between adjacent polymers π-orbitals, π - π interactions, which to a smaller degree alters the color [27].

Polyacetylene is the simplest conjugated polymer. It is a linear chain of carbon atoms, but aromatic polymers with a ring structure, such as polythiophene, also have the alternating single and double bond "backbone" and are thus a conjugate polymer as well (Figure 11) [28].

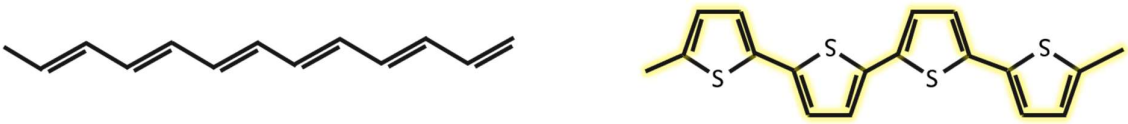

Figure 11 To the left: A linear chain of a conjugated polymer, polyacetylene. To the right: A chain of the aromatic conjugated polymer polythiophene with the alternated single-double bond backbone highlighted. To highlight the conjugation of the left polymer, polyacetylene, is left as an exercise to the reader.

By introducing available states in the bandgap, the optical spectra will shift due to absorption of lower energy photons. This is done by oxidizing, or p-dope, the polymer. The traditional picture of the oxidation process is that by removing an electron from the polymer a *polaron* is generated in the polymer chain. A polaron is a charge trapped in the potential well created by itself. This is also called a radical cation and it is localized on the polymer chain. Two new allowed states (*bonding* and *antibonding*) are created in the bandgap and the bonding is occupied by the polaron - a half-filled state. Further oxidation will generate a second polaron or, in some cases, a bipolaron/dication. The generation of a bipolaron can happen if the polymer is already highly doped. The bipolaron shifts the allowed states in the bandgap further from the band edges and is, in the case of p-doping, not occupied[27, 29].

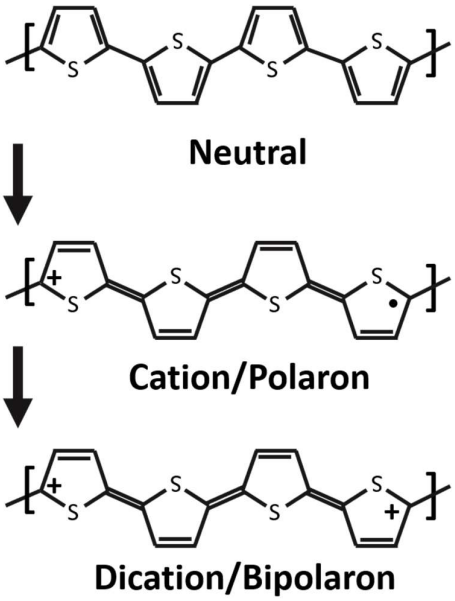

Figure 12 Oxidation of polythiophene from neutral (top) to creation of a polaron (middle) and finally a bipolaron (bottom).

An example of oxidation of polythiophene is shown in Figure 12 where the top molecule chain is the neutral polymer that gets oxidized and a polaron localized over 4 monomers forms. The bottom structure displays a bipolaron [27-29]. To balance out the charged sites on the polymer, negatively charged anions are present to form a polymer-ion complex [27].

There is a structural change accompanying the oxidation which distorts the lattice. This distortion of the lattice creates the potential well required for a polaron to be formed [27, 29, 30]. Figure 13 displays a schematic of the band structures of a conjugated polymer which goes through the process of oxidation with polaron and bipolaron formation. A schematic of the absorption spectra for different grades of doping is displayed to the right in the same figure.

A polymer with a high bandgap in its neutral state is called anodically coloring since its oxidized state is colored; polypyrrole is an example of this. A lower bandgap is called cathodically coloring since its reduced (neutral) state is colored; thiophenes are examples of this [31].

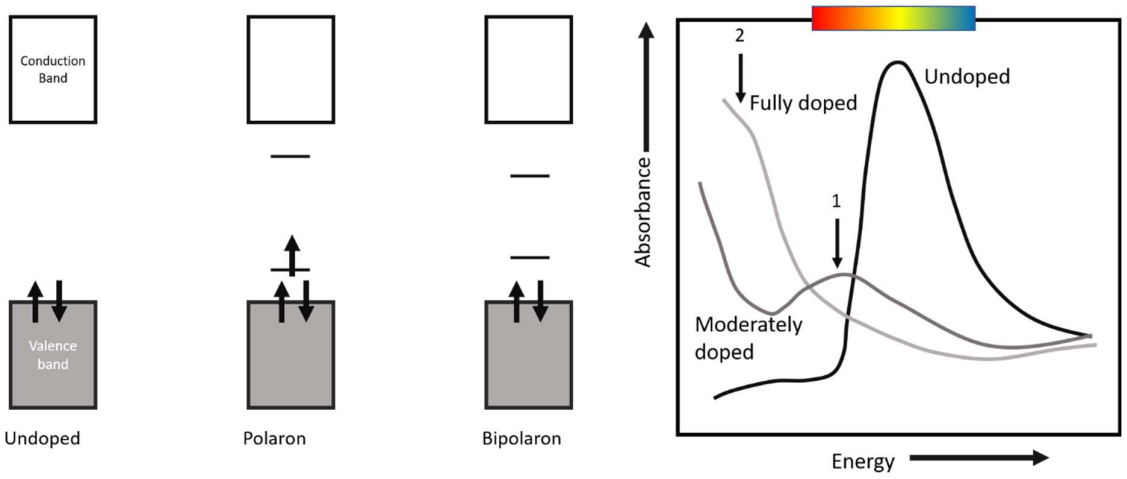

Figure 13 To the left: The traditional band structure for the undoped (neutral) polymer, a polaron, and the bipolaron. To the right: Absorbance of an undoped, moderately doped, and fully doped polymer. The two different states of doping do not strictly correspond to the polaron and bipolaron. Two absorption peaks are pointed out with arrows.

Even though the picture of a distinct polaron and bipolaron formation have been used for the past decades it has recently been challenged using more modern computational experiments such as density functional theory (DFT). Previously the absorption peak with lower energy which occurs at moderate doping, peak 1 in Figure 13, has been assigned to be the polaron formation and the second peak (2), with lower energy which occurs at further doping, has been assigned to be the bipolaron formation. By doing DFT calculations on oligomers of PEDOT, Zozoulenko et al. [32] demonstrated that the picture seems to be more nuanced. Both polaron and bipolaron absorption can be assigned to the first peak and the same is true for the second peak with lower energy. The band structure of a polarons have also been challenged with instead of having a half-filled state in the band gap it is unfilled [32].

Many conjugated polymers exhibit electrochromism, and an extensive amount of effort has been put down to create a variety of different polymers which are able to switch between various colors [33].

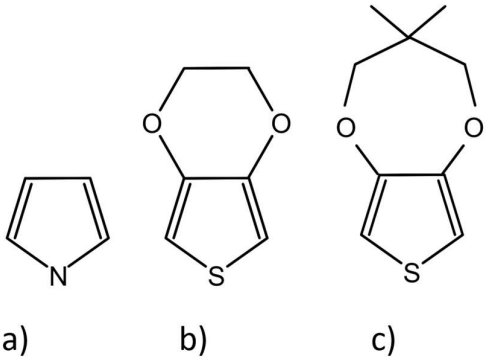

Figure 14 Structures of monomer: a) PPy, b) EDOT and c) ProDOT-Me$_2$.

Three different polymers are used in this work: Polypyrrole (PPy), poly(ethylenedioxythiophene) (PEDOT) and poly(dimethyl-propylenedioxidethiophene) (PProDOT-Me$_2$). The monomers can be viewed in Figure 14.

PEDOT and PProDOT-Me$_2$ are cathodically coloring electrochromic materials where PProDOT-Me$_2$ have higher optical contrast and faster *switching time* (time required for a color-switch). The faster switch of PProDOT-Me$_2$ can be attributed to the more open morphology which facilitates faster intercalation of counterions [34]. The spectral range in which the absorption occurs is also broader for ProDOT-Me$_2$ since it has split vibration mode, giving it two absorption peaks [35-37].

There are various methods of depositing polymers on a surface. Various printing processes such as inkjet, screen printing, and spray coating can be used to manufacture large areas [38]. The polymer must already be synthesized in these cases. Synthesizing the polymer from the monomer directly on a surface can be done with either vapor phase polymerization [39] or electropolymerization. The latter is used in **Paper I** and **Paper II**. In **Paper III,** screen printed PEDOT:PSS (PEDOT polymerized with polystyrenesulfonate as dopant) was used because it does not require a conductive substrate for electrochromic applications [40, 41].

Electropolymerization is done by elevating the potential of an electrode above a certain threshold. One reaction scheme is of how the polymer is produced is the *Diaz's mechanism*. A monomer in the solution gets oxidized, and a radical of the monomer is formed. A dimer of two radical monomers is made by producing a covalent bond between the unpaired electron pairs and successively lose two protons. The process is repeated by oxidizing the dimer, which in turn bonds with a radical monomer similarly, the schematic can be seen in Figure 15 [42]. The unpaired electron pair is delocalized over the monomer, so for some monomers, such as pyrrole or thiophene, the covalent bond between the radical monomer and the dimer could be forming at several positions, creating a branched chain [43].

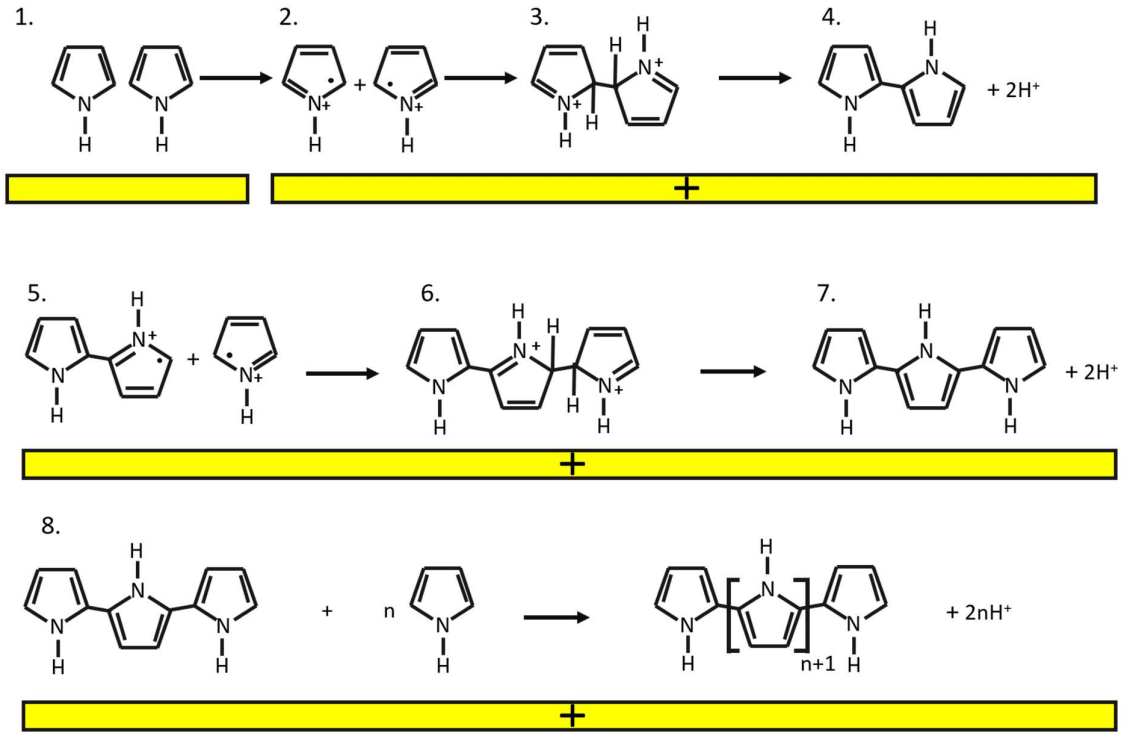

Figure 15 1.) Monomer in the electrolyte. 2.) A radical is produced on the monomer when an anodic potential is applied to the electrode. 3.) A covalent bond is produced between two monomers with radicals to create a dimer 4.) Two protons are leaving to stabilize the dimer. 5.) The dimer can be oxidized in the same manner as the monomer and react with a radical monomer 6.) A trimer is created 7.) Two protons are leaving the trimer 8.) The process is repeated with more monomers until a polymer is produced.

The total growth process is not entirely understood, but it is suggested that it includes three different stages: 1) Soluble oligomers are formed in the *diffusion layer*, the distance in the vicinity of the electrode where the concentration differs from the bulk concentration. 2) Deposition of the oligomers by nucleation and growth processes. 3) Solid state polymerization where longer chains are produced [44].

The polymerization potential is above the oxidation potential for the polymer which leaves the polymer in an oxidized state after the polymerization. Anions are present to balance out the charged polymer [44].

By reducing the polymer electrochemically in an electrolyte, the polymer becomes neutrally charged. Both intercalating cations and de-intercalating anions can facilitate charge neutrality. What happens depends on the size of the anion used while producing the polymer. If it is big and bulky, it will be stuck, and cation ingress is easier for reaching charge neutrality. If the anion is small, anion egress is easier for reaching charge neutrality [44]. The two cases, cation and anion -doping is displayed in Figure 16. For polypyrrole in aqueous electrolyte, dodecylbenzenesulfonate (DBS^-) and tosylate (Tos^-) are examples of anions that will get stuck and generate a cation doping. Perchlorate (ClO_4^-) and hexafluorophosphate (PF_6^-) are ions that will undergo anion doping [45]. The moving of ions in and out of the polymer causes the film to change volume. Therefore are conjugated polymers investigated to be used as microactuators [43] and artificial muscles [46].

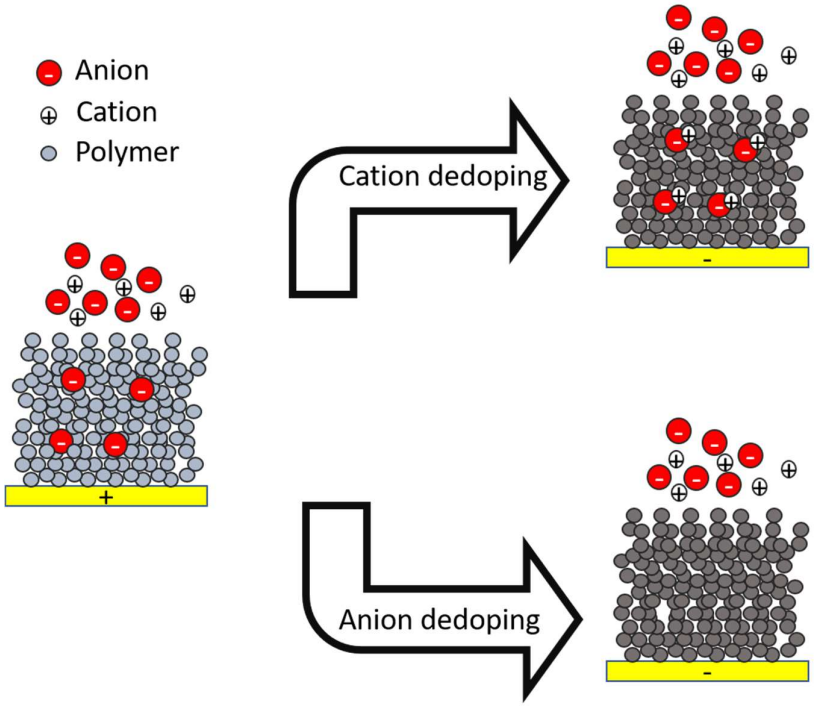

Figure 16 A schematic of the two different doping processes that can occur. To the left is the oxidized/doped polymer with negatively charged anions intercalated into the polymer matrix. When reducing the polymer to neutral the negatively anions charge can be compensated by intercalation of positively charged cations. This route is indicated by the top arrow. The negatively charged anions can also be expelled from the polymer matrix to get charge neutrality. This route is indicated by the lower arrow. The red circles represent the anions, the white circles represent the cations and the grey/dark grey circles represent the polymer. The change from light to dark grey represents the electrochromic effect. The features are not drawn to scale.

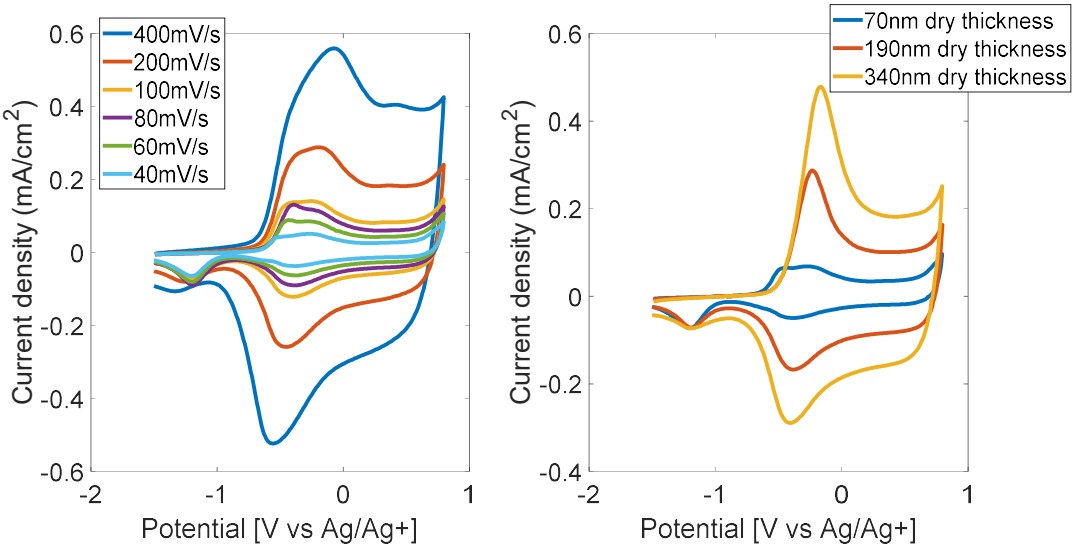

Figure 17 To the left: CV diagrams of a PProDOT-Me_2 film on 20 nm gold with varying scan rate, 70 nm dry thickness. To the right: CV diagrams of three different thicknesses of PProDOT-Me_2 on 20 nm gold with a scan rate of 100 mV/s. CV diagram collected by yours truly, the author.

The electrochemistry of the doping and dedoping of conjugated polymers are rather complex and beyond the scope of this thesis. However, a brief summary of some models will be presented.

If assuming a pure *faradic reaction* of the adsorbed polymer and no diffusion the CV diagram would look like Figure 7. However, there is an additional box-like behavior at potentials slightly above the peak current which indicates that there is a capacitive behavior (Figure 17). The theory of adsorbed analytes is only valid for the boundary and the polymer is not regarded as a boundary because, in some instances, the thickness is in the micrometer regime it.

A capacitive element can be added to make up for the plateau region and the CV [47], but the capacitive region is not the only phenomena that cannot be explained by the simple theory of surface adsorbed species. When applying an anodic potential from a cathodic potential to polypyrrole in $LiClO_4$ the current starts out small but increases for some time until it drops of again. More advanced methods introduce *conformational relaxation* - energy and time required to alter the structure of the polymer. The structural changes generate the current delay and better models the chronoamperograms. According to the theory of this method the doping is done in four steps: 1) Positive charge formation on the polymer. 2) Changes in the polymer matrix, the conformational relaxation. 3) Diffusion of counterions into the polymer. 4) Additional exchanges such as solvents and *ion pairs* (non-solvated ions) [48]. The system of PPy:Tos (tosylate) in $LiClO_4$ displays 'shoulders' in the cathodic chronoamperogram which is attributed to the opening up of the polymer for cation ingress [49]. This theory have been named ESCR model, electrochemically stimulated conformational relaxation [45] and have been further improved by adding migration, ion movement due to an electric field [50].

The ion movement in PEDOT:PSS have been modeled without using any electrochemical reactions but only *the Nernst-Planck-Poisson equation*, the Nernst-Planck with the *Poisson equation* – a relation between charge density and electric potential. Both one phase model, PEDOT:PSS as one material, and a two phase model, PEDOT and PSS in different branches, was modeled and could simulate the CV diagram well [51].

One of the drawbacks of conjugated polymers is their lifetime. After many switching cycles, it will eventually degrade, but under certain conditions, some polymers have cycle durability of the order of one million switches [52], something which is further improved in **Paper I**. One reason for its degradation is said to be delamination due to stress build-up in the polymer substrate interface due to volume change in the polymer [53] another is overoxidation of the polymer, leaving it non-functional [54, 55].

2.4 Spectroelectrochemistry

By measuring the transmission simultaneously as various voltages are applied to the electrochromic material the contrast can be measured. Contrast can be defined as the difference in either transmission or reflection of the bleached (ble) and the colored (col) state.

$$\Delta T = T_{ble} - T_{col} \quad (17)$$

If the electrochromic film and the electrolyte have fairly similar refractive indices no additional reflection needs to be taken into account, and the polymer film is expected to follow Lambert-Beer law where the absorption is proportional to the thickness (t), the concentration of absorption sites (c) and the molar extinction (a). If the absorption sites of the polymer don't scatter light the optical extinction is equal to the absorption. Two equations, Equation 18 and 19, that connect the transmission to the thickness of the film can then be assigned, one for the colored state and one for the bleached state. Equation 20 displays how the transmission difference depends on the thickness.

$$E_{col} = a_{col} c t = -\log(T_{col}) \quad (18)$$

$$E_{ble} = a_{ble} c t = -\log(T_{ble}) \quad (19)$$

$$\Delta T = e^{a_{ble} c\, t} - e^{a_{col} c\, t} \quad (20)$$

By converting both to transmission and taking the difference, the thickness-dependent contrast will be obtained. Visualization of Equation 18 and 19 can be viewed to the left in Figure 18. The transmission from Equation 18 and 19 can be seen to the right in Figure 18 together with Equation 20.

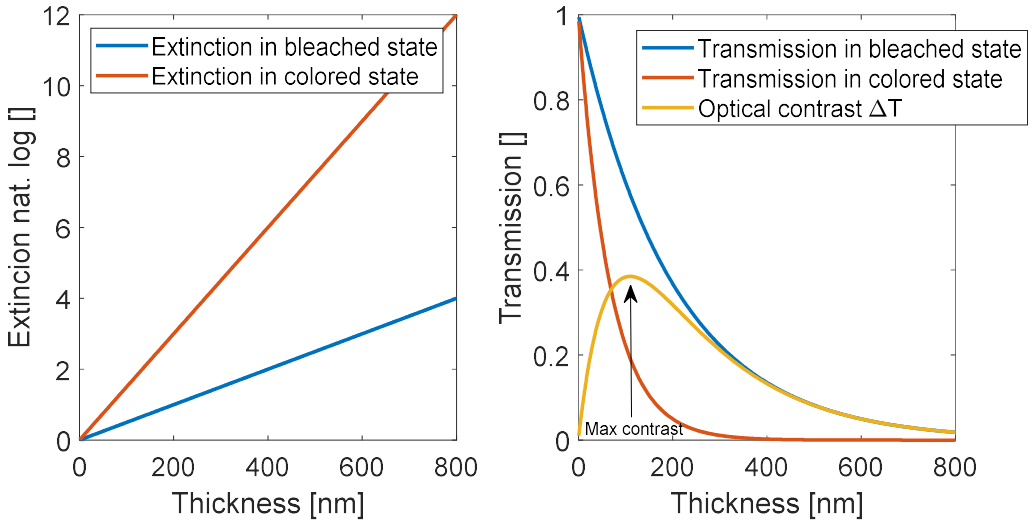

Figure 18 To the left: Equations 18 and 19 are visualized. Optical extinction plotted against thickness for two different values of molar extinction coefficient a_{ble} =0.05 [mM^{-1} nm^{-1}] a_{col}= 0.015 [mM^{-1} nm^{-1}]. The concentration of absorption sites is set to 1 mM. To the right: The transmission of Equation 18 and 19 plotted against thickness together with the transmission difference, Equation 20. The arrow indicates the maximum contrast. The values for the concentration and the molar extinction coefficients are hypothetical examples.

Analytically finding the thickness which corresponds to the maximum contrast can be done by taking the derivative of the contrast and assign it zero, then solving for the thickness. This is done in Equation 21 to 25. By inserting the optimal thickness in the contrast equation (Equation 20), a formula for the maximum contrast will be obtained. This is done in Equation 26 to 29.

$$\frac{d\Delta T}{dt} = a_{ble} c\, e^{a_{ble} c\, t_{max}} - a_{col} c\, e^{a_{col} c\, t_{max}} = 0 \qquad 21$$

$$a_{ble} c\, e^{a_{ble} c\, t_{max}} = a_{col} c\, e^{a_{col} c\, t_{max}} \qquad 22$$

$$\frac{a_{col}}{a_{ble}} = e^{-(a_{col}-a_{ble}) c\, t_{max}} \qquad 23$$

$$\log\left(\frac{a_{col}}{a_{ble}}\right) = -(a_{col}-a_{ble}) c\, t_{max} \qquad 24$$

$$\frac{-\log\left(\frac{a_{col}}{a_{ble}}\right)}{(a_{col}-a_{ble})c} = t_{max} \qquad 25$$

$$\Delta T_{max} = e^{a_{ble} c\, t_{max}} - e^{a_{col} c\, t_{max}} \qquad 26$$

$$\Delta T_{max} = \exp\left(-a_{ble} \frac{\ln\left(\frac{a_{col}}{a_{ble}}\right)}{(a_{col}-a_{ble})}\right) - \exp\left(-a_{col} \frac{\ln\left(\frac{a_{col}}{a_{ble}}\right)}{(a_{col}-a_{ble})}\right) \qquad 27$$

$$\Delta T_{max} = \left(\frac{a_{col}}{a_{ble}}\right)^{-\frac{a_{ble}}{(a_{col}-a_{ble})}} - \left(\frac{a_{col}}{a_{ble}}\right)^{-\frac{a_{col}}{(a_{col}-a_{ble})}} \qquad 28$$

$$\Delta T_{max} = \left(\frac{a_{col}}{a_{ble}}\right)^{\frac{1}{(1-\frac{a_{col}}{a_{ble}})}} - \left(\frac{a_{col}}{a_{ble}}\right)^{\frac{\frac{a_{col}}{a_{ble}}}{(1-\frac{a_{col}}{a_{ble}})}} \qquad 29$$

From the above derivation, the maximum contrast is only governed by the ratio of the material's molar extinction coefficients in the colored and the bright state. If the concentration and thickness are the same in both states, this ratio is equal to the optical extinction ratio obtained by two transmission measurements. Previous work has shown the validity of this method for conjugated polymers by observing that the optical extinction is linear with the thickness and that there is an ultimate thickness for the best contrast [56].

Besides contrast, another important factor is the switching time, usually defined as the time to reach 95% of the complete contrast after a potential is applied. It is desirable to have a low switching time. It is also desirable to have a long bistability or retention time, which is the time the material remains in its state after the potential have been removed.

3 Methods

3.1 Plasmonic metasurfaces

The plasmonic color pixels are made by depositing a silver or an aluminum mirror on glass. The deposition technique used is physical vapor deposition, and ~100 nm is deposited. The spacer layer, aluminum oxide, is evaporated directly on top of the mirror. The thicknesses used in this work are 61 nm for red, 110 nm for green, and 95 nm for blue. For the red pixel, the plasmonic effect is not desired since it scatters red light and decreases the reflection in this spectral region, and 20 nm of gold is evaporated directly on top of the aluminum oxide, but for the green and blue pixel, colloidal lithography is used to generate a hole-array in the gold.

3.2 Spectroscopic measurement

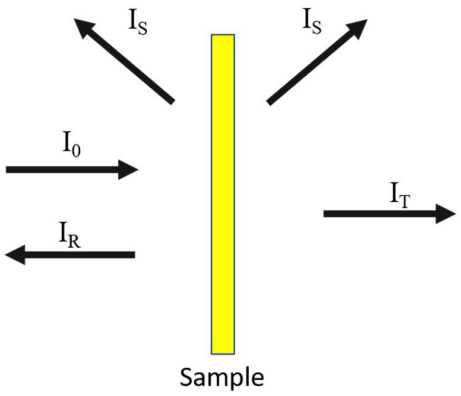

Figure 19 Schematic of light with the intensity I_0 hitting a sample.

When light hits a sample, reflection, transmission, scattering and absorption can occur (Figure 19). For monochromatic light, the transmission is defined as the ratio of the light intensity of the transmitted light and the incident light, $T=\frac{I_T}{I_0}$. The reflection is defined as the ratio of the reflected intensity and the intensity of the incident light, $R=\frac{I_R}{I_0}$.

Optical extinction is defined as $E=-\log\frac{1}{T}$ and is the total attenuation, including reflection, absorption, and scattering. If reflection and scattering are small optical extinction can be approximated to the absorbance of the sample.

The spectroscopic setup for transmission measurements is as follows:

1. A fiber optical cable is used to guide the light from a light source (Azpect Photonics),
2. The light is collimated
3. The sample is illuminated
4. The transmitted light is collected by an objective (4x / NA 0.1)
5. The light passes through a focusing lens.
6. The light is split in a beam splitter
7. One portion of the light is guided by a fiber optical cable into the spectrometer (B&WTek)
8. The rest of the light is once again split.
9. The light is collected by a camera.

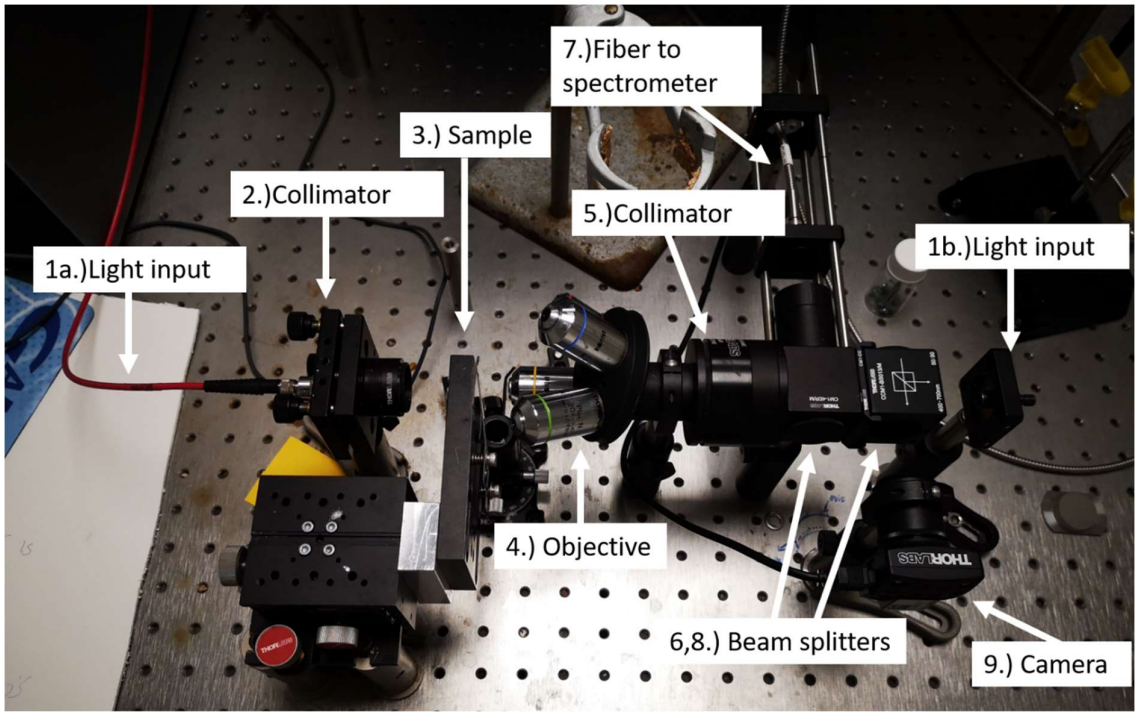

Figure 20 A picture of the reflection/ transmission setup, here in transmission mode.

A reference spectrum is measured without the sample and the transmission is obtained by dividing the sample spectrum by the reference. The spectrum and the reference spectrum have a dark spectrum subtracted from them, which is the intensity with no light source (Equation 30).

$$T=\frac{I_{sample}-I_{dark}}{I_{reference}-I_{dark}} \qquad 30$$

Reflection measurements are made similarly, but the fiber optical cable is attached to the rightmost input (1b in Figure 20), and the sample is illuminated through the objective. The reference is a commercial dielectric silver mirror (BB05-E02, Thorlabs) which reflects nearly 100% in the visible regime.

The reflection can also be measured by illuminating the sample with diffuse light produced by an integrating sphere (Konica Minolta CM-700d), schematic in Figure 21. This configuration is used to measure the reflection of the pristine metasurfaces [57].

1. The integrated sphere is illuminated by the light. A baffle is included to block the light to radiate the sample directly.
2. The light is reflected from the surface of the integrating sphere and produces *diffuse light*, not collimated light, which illuminates the sample from all angles.
3. The reflection from the sample is collected by a photodetector at an angle of 8° to the normal of the sample.
    a. If the light trap is shut, Figure 21 to the left, the sample is *also* radiated with the light 8° from the normal. Thus, making it a *specular reflection* to the spectrometer. This configuration is referred to as (di/8).

b. If the light trap is open, Figure 21 to the right, the *specular reflection* is excluded from the measurement. This configuration is referred to as (de/8)

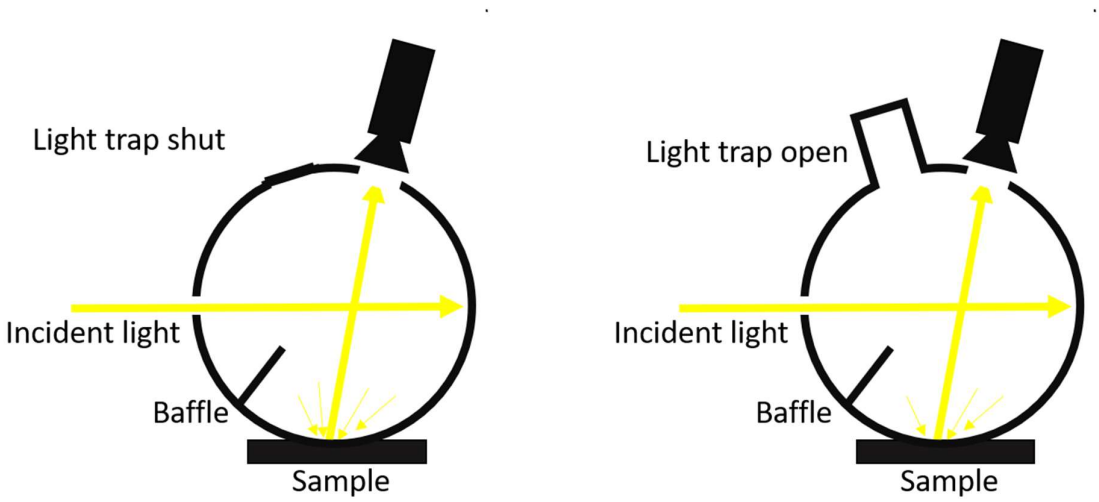

Figure 21 Schematic of an integrated sphere setup in (di/8) configuration (to the left) and in (de/8) configuration (to the right). In both configurations' incident light is illuminating the integrated sphere which produces diffuse light. The sample is illuminated with diffuse light and the reflection is measured.

To qualify the luminosity (brightness) and the chromaticity (saturation) of a sample, the spectrum is converted to the *CIE 1931 color space*. The procedure of doing this is to multiply the spectrum, $\mathrm{R}(\lambda)$ or $\mathrm{T}(\lambda)$, with a *color matching function* which represents the eyes' sensitivity to different wavelengths of light. There are three different *color matching function:* $\bar{\mathrm{x}}$, $\bar{\mathrm{y}}$ and $\bar{\mathrm{z}}$, which all spans different parts of the visible spectrum.

The spectrum with the color matching function is integrated over the visible wavelengths (360 nm to 740 nm) and normalized with the color matching function $\bar{\mathrm{y}}$ integrated over the same wavelength span. This generates three different values; X, Y and Z, also known as the *tristimulus values* where Y is an indication of how luminous (bright) the color is. Equation 31 shows how calculation of X is done for reflected light. The remaining, Y and Z, is done analogously. In some cases, the color matching functions are multiplied with a *standard illuminant*, a spectrum which contains the information of which lighting conditions the sample is in.

$$\mathrm{X} = \frac{\int_{\lambda=360\mathrm{nm}}^{740\mathrm{nm}} \mathrm{R}(\lambda)\,\bar{\mathrm{x}}(\lambda)\,\mathrm{d}\lambda}{\int_{\lambda=360\mathrm{nm}}^{740\mathrm{nm}} \bar{\mathrm{y}}(\lambda)\,\mathrm{d}\lambda} \qquad 31$$

To quantify the chromaticity of the spectra the tristimulus values X and Y is normalized to the sum of all three tristimulus values X+Y+Z to generate *x* and *y* (not to be confused with $\bar{x}, \bar{y}$ and $\bar{z}$) (Equation 32 and 33). Plotting the *x* and *y* in a *xy-graph* the chromaticity can be viewed.

$$x = \frac{X}{X+Y+Z} \tag{32}$$

$$y = \frac{Y}{X+Y+Z} \tag{33}$$

Any point close to the *white point* (a defined point in the diagram which represents white) indicates a less saturated color while a value further from the white point (closer to the edges) indicates a more saturated color. An example of this can be seen in Figure 22 where two normal distributions centered around 550 nm acts as example spectra. A broader reflection peak (-) is closer to the white point and thus has a less saturated color than the narrower peak (--). What must be considered is the overall reflection is higher for the broader peak (Y=74) than for the narrow peak (Y=42) [58, 59].

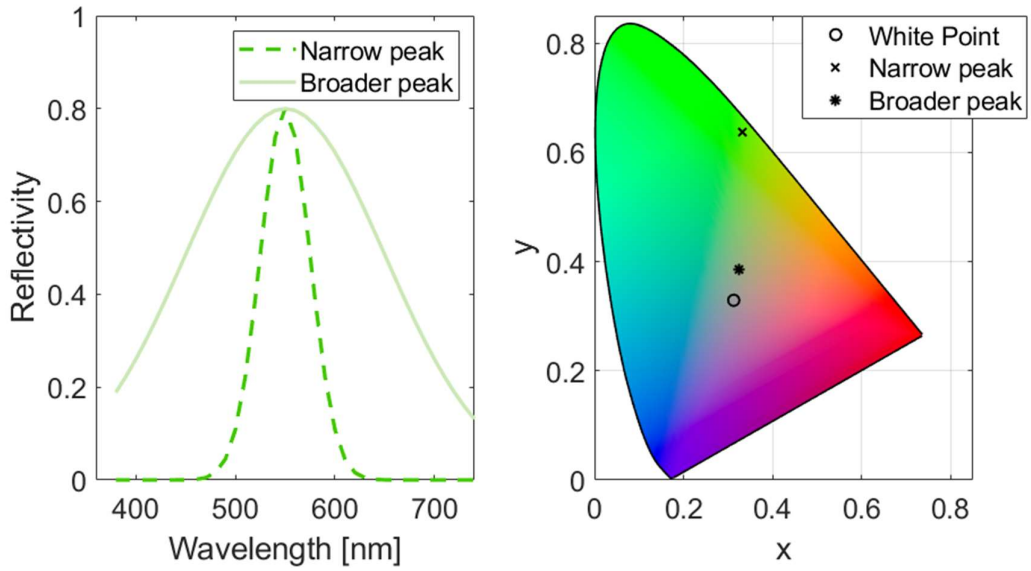

Figure 22 To the left: Two computer-generated example spectra centered around 550 nm. A narrower peak (--) reflects less light while the broader peak (-) reflects more light. The color of the spectra lines is the corresponding 'pseudo-colors' for the spectra generated by converting the XYZ values to sRGB. To the right: Corresponding xy-graph for the spectra to the left with the white point (o). Note the narrow peaks point (X) is further from the white point than the broader peak (*) thus have a higher chromaticity.

3.3 Electrochemistry

It is essential to be able to control the applied potential and measure the correct passed current. A widespread electrochemical setup is a *three-electrode setup*, which is used to analyze processes at an electrode. The setup consists of one working electrode (WE) where the reaction takes place, one reference (Ref.) against which the potential is measured, and one counter electrode (CE), which ideally acts as an electron reservoir (Figure 23).

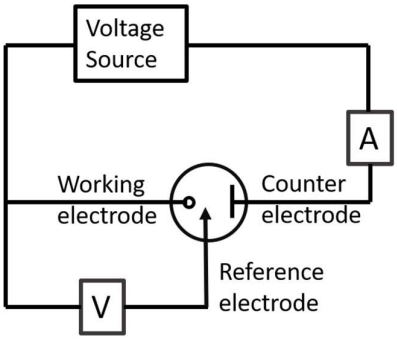

Figure 23 A schematic of a three-electrode setup.

The working electrode is usually an inert metal such as platinum or gold, but it can also be made of carbon or transparent conductive material such as ITO. Since the top layer of the metasurfaces is 20 nm of gold the working electrode in this study is mainly 20 nm of gold on glass. The reference electrode should have a fixed potential between the electrolyte and the electrode. For example, the reference electrode could consist of lithium metal in a solution of lithium ion containing electrolyte, or a silver wire immersed in a solution with silver ions. The latter is utilized in this work.

The counter electrode is present to close the circuit and donate or accept electrons into the electrolyte. No voltage is measured on this electrode. A platinum coil with a four times larger area than the working electrode is used in this work.

The equipment called *potentiostat* controls the three-electrode setup with preprogrammed experiments: Chronoamperometry measures a current with a constant applied potential. If the polymerization-potential is known, this potential could be applied directly to the working electrode to synthesize the conjugated polymer from the monomer. In this work CV it is used to deposit the polymer on top of the electrode by sweeping from a negative potential towards a potential slightly higher than the polymerization potential. All measurements were made with a Gamry Interface 1000/1010E.

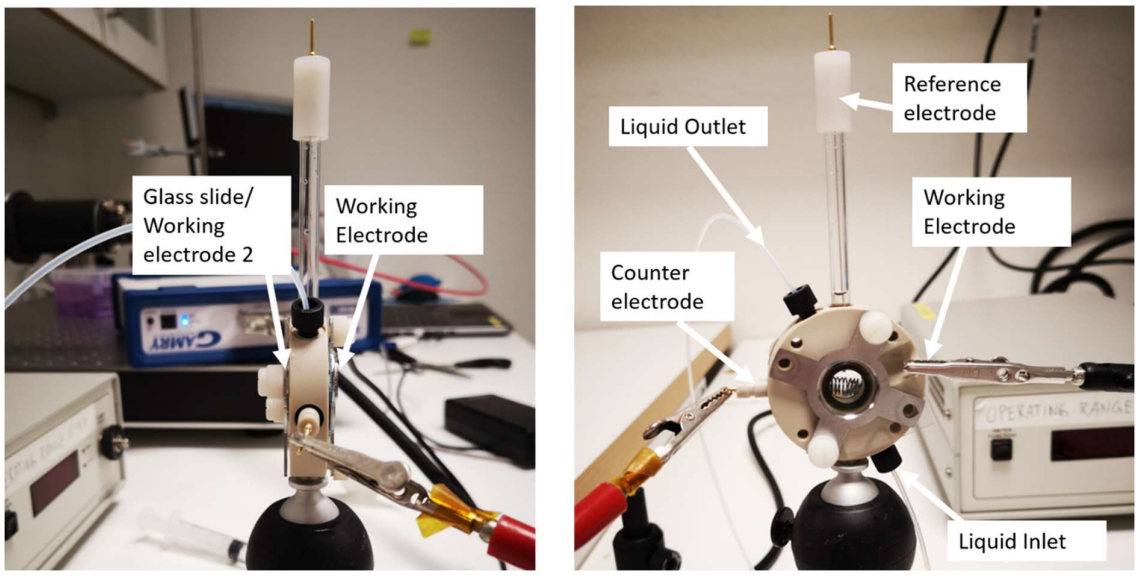

Figure 24 Electrochemical flow cell for spectroscopic measurements.

The measurements were made in a custom-made electrochemical flow cell (Figure 24) with a hollow compartment where the liquid is contained by two glass slides. One of the slides is a glass window, and the other slide supports the sample, also acting as the working electrode. This facilitates spectroscopical measurements, both transmission and reflection, measured simultaneously with the electrochemistry. The reference electrode is a commercial Ag/Ag+ reference that consists of a silver wire immersed in 0.1 M tetrabutylammonium perchlorate and 10 mM silver nitrate in acetonitrile separated from the cell electrolyte with a ceramic frit. The counter electrode is a platinum coil. In transmission mode, the optical extinction of the flow cell and the gold substrate was subtracted to the measured optical extinction to get only the contribution of the polymer.

In reflection measurements, to account for the flow cell's absorptive contribution, a homemade silver mirror was measured in the flow cell filled with electrolyte. The homemade mirror was later measured in air and the reflectivity was compared to the commercial dielectric mirror. The electrochemical cell with the reference and counter electrode was purchased by Redoxme AB. In **Paper I** a similar flow cell was used with a reference electrode made of a silver wire coated with silver chloride (Ag/AgCl).

4 Results

4.1 Color pixels

Silver is currently the best material to use as the bottom mirror because of its high reflection. However, the silver is not stable in the organic solvents with the electric potential required to switch the electrochromic materials. Aluminum was instead used to overcome this issue.

The reflectivity of the spectra of red, green, and blue pixels measured with the diffuse light in the integrated sphere configuration (di/8) was around 0.8 (Figure 1A in **Paper II**). The thicknesses of the spacer layer were 65, 110, and 95 nm, respectively. The scattering due to the plasmons was located in the spectrum's red region (Figure 1D in **Paper II**). The nanohole-array was then omitted for the red pixels to avoid decreasing the reflection.

In **Paper I**, the colloidal particles were not stripped away from beneath the gold top reflector on the green and blue metasurfaces creating a structure with positive curvature (Figure 1a in **Paper I**). The red pixel used gold as both bottom mirror and spacer layer and the red coloration was produced by the absorption of the gold and the plasmonic effect.

Copper was used in **Paper III** instead of gold as the top electrode. However, copper oxidizes in ambient air, so a protective coating was deposited. This coating was non-conductive, which did not allow electropolymerization to be performed. PEDOT:PSS was used as the electrochromic material since it does not require an electrically conductive substrate due to its high conductivity.

Going back to the first paper on the topic published by Kunli et al. in 2016 using a silver-alumina-gold structure [8] and comparing it the later structures, aluminum-alumina-copper, **Paper III,** or the aluminum-alumina-gold, **Paper II**, the structures with silver as a back reflector outperforms the aluminum reflector for green and blue in terms of highest reflection. The metasurface with copper as a top layer has highest reflection for red samples.

4.2 Electrochromic conjugated polymers

One of the polymers which have the highest reported contrast is PProDOT-Me_2 and it was one of the scopes to investigate this electrochromic material in **Paper II.** Two different solvents were used together with various salts to get a uniform film of the polymer on a 20 nm gold film. When acetonitrile was used as a solvent it seemed like the gold film degraded at similar potential required to polymerize ProDOT-Me_2. It is described in the literature that acetonitrile might not be the best choice for electropolymerization due to its low basicity [44].

PProDOT-Me_2 has previously been polymerized on porous gold [60, 61] and electroless gold [62] with propylene carbonate. This solvent indeed gave better results. Various deposition methods were used as well: constant potential, constant current, and cyclic voltammetry. For our setup, cyclic voltammetry gave the most reliable results where different methods gave various uniformities of the film (Figure S2 in **Paper II**).

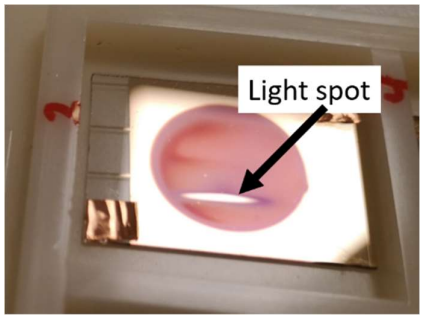

Figure 25 PProDOT-Me_2 polymerized on gold while illuminated.

It should be noted that both constant potential and constant current sometimes gave good uniformities in both propylene carbonate and acetonitrile, but the method which gave the most stable reproducibility was cyclic voltammetry with propylene carbonate as the solvent. One reason for this could be that diffusion is faster in acetonitrile than propylene carbonate and the polymerization occurs at a higher rate. Previous studies on PPy have described the potentiostatic method (chronoamperometry) to grow a more branched tree-like structure (dendritic) on platinum in acetonitrile, while cyclic voltammetry gives a smooth uniform layer [63]. This could be the reason that cyclic voltammetry gives better uniformity in our setup. The scan rate of the produced film displayed a linear relationship with the peak currents which agrees with the theory of surface adsorbed layers and/or the theory of capacitive currents as described in previous section and displayed in Figure 7 and Figure 8.

It was noticed that when polymerization was tried in the transmission setup with a light spot on the gold substrate, the polymer would not deposit at the illumination spot (Figure 25). This interference made it impossible to measure the optical properties simultaneously with the deposition. Using cyclic voltammetry, the light could be shut off during the polymerization sweep and turned on after the sweep. This made it possible to measure the optical extinction of reduced (pristine) polymer between every growth cycle.

The charge transfer, the integrated current of one deposition cycle, is linear with the number of polymerization cycles (Figure 2A in **Paper II**). This will correspond to the amount of charge consumed to oxide the monomer (2 electrons per monomer). If all oxidized monomer contributes to building up the polymer-chain, the optical extinction should be linear with the charge transfer. In Figure 26 the optical extinction is plotted against the number of polymerization cycles, and it is clear that the relationship is not perfectly linear. The decline in the optical extinction can be attributed to the fact that not all polymer adheres to the surface, but some are still soluble in the solvent and are sinking down to the bottom in the flow cell. Thus, they are not observed in the optical measurement.

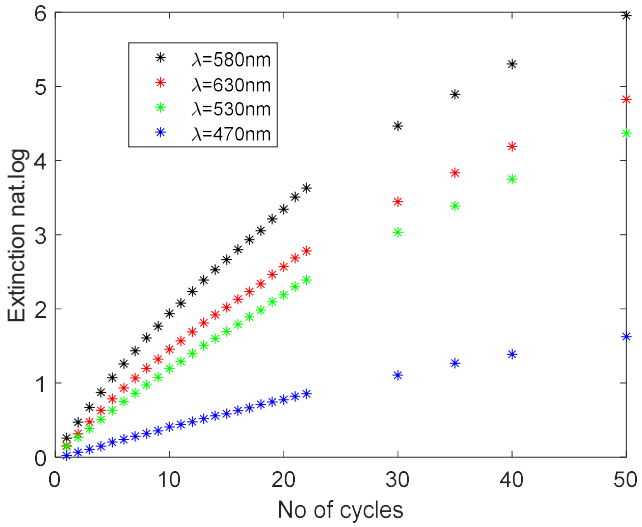

Figure 26 The optical extinction of PProDOT-Me_2 with the number of polymerization cycles.

The polymerization voltage, ~1.1 V vs. Ag/Ag+ is above the voltage required to reach the maximum contrast of PProDOT-Me_2 during switching from colored to bleached state, -1V and +0.5V vs. Ag/Ag+. The polymerization with CVs can be paused and measurements can be done to find transmission in colored and bleached state and thus the contrast corresponding to that thickness. This is done to visibly see that there is an optimal thickness that gives a maximum contrast of the polymer (Figure 2D **Paper II**).

To further validate that the method of finding the maximum contrast of an electrochromic material by just measuring the optical extinction ratio, the ratio was measured for different thicknesses and it was confirmed that it was constant (Figure 3A in **Paper II**). Two other polymers, polypyrrole (PPy) and polyethylenedioxythiophene (PEDOT) were also evaluated and the optical extinction ratio of the three tested polymers were compared. PProDOT-Me_2, with its high optical extinction ratio, has the highest contrast (~78% at 580nm) (Figure 3A in **Paper II**).

The dry thickness was measured with a profilometer, and the thickness vs charge consumption was in agreement with previously reported values of a similar polymer that was deposited using a potentiostatic method [35] (Figure S3 in **Paper II**). Polymerization of PProDOT-Me_2 on the plasmonic metasurfaces was made in the same fashion as on the 20 nm gold films. The contrast was between 50% -60% for the samples, red, green, and blue (Figure 4A **Paper II**). The lowest contrast is for blue. Implementing other polymers such as poly(propylenedioxypyrrole) (PProDOP) could be beneficial to increase the contrast in the blue regime [64].

The structures were patterned into stripes to mimic how the color would appear in a device utilizing red, green, and blue subpixels (Figure 1D in **Paper II**). PProDOT-Me_2 was deposited on the blue and switched on and off. Results can be seen in the supplementary video to **Paper II** and the front cover of this thesis.

In **Paper II,** electropolymerization on the positive-curvature structures was made in propylene carbonate with cyclic voltammetry in the same fashion. Electropolymerization was not possible in **Paper III** since the structure had a protective dielectric coating. PEDOT:PSS was instead screen

printed on top of the protective coating and acted as the electrochromic material and electrical conductor. The contrast of the PEDOT:PSS structures was between 30% - 40% (Figure 4 in **Paper III**).

Switching speed is one important factor that should be considered when choosing the electrochromic material. For polymers such as PProDOT-Me_2 the switching speed is usually less than 1 s, depending on the thickness of the sample.

The potential is also a contributing factor where more extreme potentials decrease the switching time. Figure 27 displays how a film of PProDOT-Me_2 switches from bright to dark, or dark to bright. It is clear that using more extreme potentials increases the switching speed (decreasing switching time). However, potentials above +0.5 V vs. Ag/Ag+ degraded the polymer since reducing it back to the same low transmission was not possible.

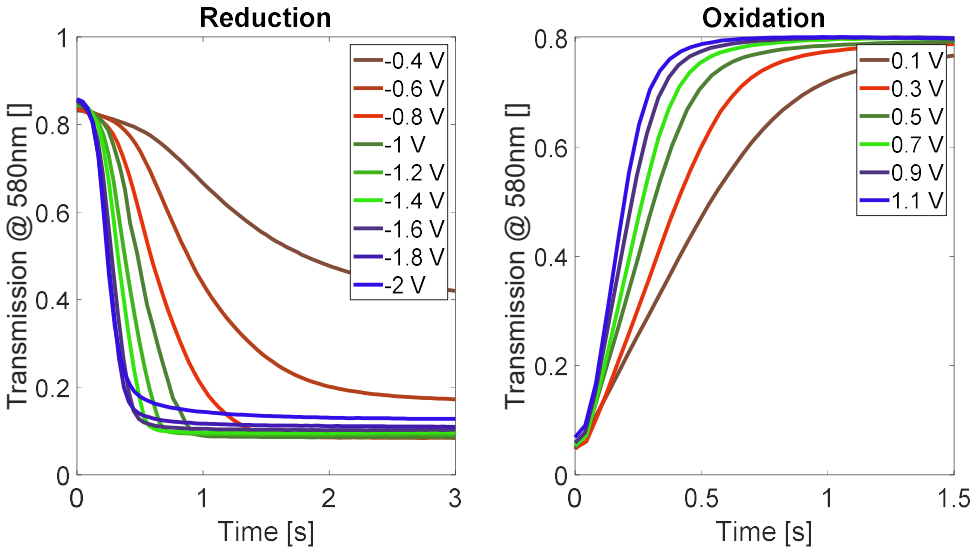

Figure 27 Transmission over time when various potentials are applied. To the left: From bleached state (+0.5 V vs Ag/Ag+) to colored state. To the right: From a colored state (-1 V vs. Ag/Ag+) to the bleached state. All potentials are against Ag/Ag+.

In **Paper I**, the possibility of reducing the switching time is investigated with great success. Changing the solvent from propylene carbonate to the less viscous acetonitrile reduces the time with around a factor four. Further increasing the salt concentration decreases the time even more. However, changing the cation from lithium to large TBA^+ (tetrabutyl ammoinium perchlorate) reduced the switching speed indicating that it might not only be anion doping that takes place. If cation doping is contributing in PProDOT-Me_2 with ClO_4^- it could explain the 'shoulder' seen in the cathodic chronoamperometric curves shown in Figure 28. The curves are obtained in a three-electrode setup on a flat gold surface. Otero et Al. have previously attributed these 'shoulders' to the cation ingress when using PPy/PTS in $LiClO_4$ and propylene carbonate [49]. *Moving front experiment,* optically monitoring the oxidation front in the polymer, displays that the 'shoulder' occurs approximately when the front reaches the end of the polymer [65], which then could be attributed to the polymer being 'full' of ions.

Other studies have also described a more nuanced view of cation and anion doping by measuring the mass change during doping and dedoping. It was concluded that it was not strictly only cation or anion doping [66]. Another study on thiophenes, including PProDOT-Me_2, did similar measurements with

the result that it was a mass increase during oxidation but similarly concluded that both cations and anions are involved [67].

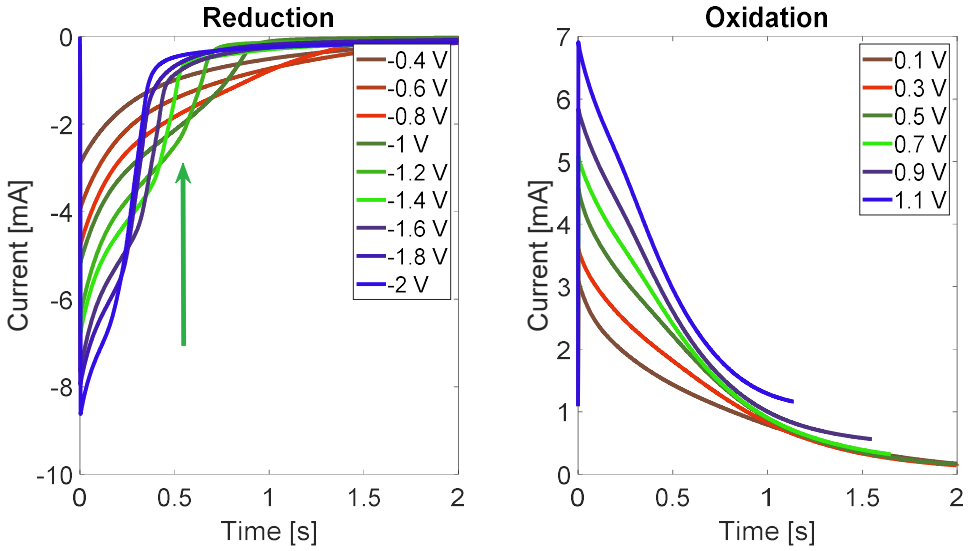

Figure 28 Current over time when various potentials are applied. To the left: From bleached state (+0.5V vs Ag/Ag+) to colored state. The arrow indicating a 'shoulder' for the potential of -1.2V. To the right: From a colored state (-1V vs. Ag/Ag+) to the bleached state. All potentials are against Ag/Ag+.

Changing the distance between the counter and the working electrode with a two-electrode setup also influenced the switching speed. Decreasing the distance from 4 mm to 0.05 mm reduced the switching time from 60 ms to 25 ms. The setup was horizontal gold electrodes with PProDOT-Me_2 on both the working and the counter electrode (Figure 2A **Paper I**). It is speculated that the results of achieving higher switching speed with a diminished distance between the counter and working electrode are due to the increased electric field which then would be the driving force moving the ions.

Assuming the concentration of 'color changing sites', intercalated ions, have a first-order kinetic response (the time derivative of the concentration is proportional to the concentration) a good fit could be obtained for the transient optical response (reflection change). This fits well with the theory of adsorbed layers which have first order-kinetics. If diffusion of the counterions into the polymer was the limiting factor the response would depend on the square root of time, similarly to the Cottrell equation.

A structured electrode surface (Figure 1a **Paper I**) was also investigated and compared to a standard planar working electrode. The switching speed is linear with the amount of deposited polymer for both electrodes, but the structured electrode generally has a lower switching time (Figure 3a **Paper I**). It is speculated that this is due to a change of the morphology of the polymer from a denser on the planar electrode to a more open on the structured electrode.

The bistability of the polymer is displayed in where a two-second pulse of -1 V vs Ag/Ag+ is applied to the is in the 100 s regime (Figure 6A **Paper II**). When using the video speed configuration (Figure 5d **Paper I**) it is seen that the coloration can be retained by applying short pulses of 20 ms every 60 s.

No lifetime measurements were made in **Paper II** or **III**. **Paper I** investigate how the number of switches influences the contrast of PProDOT-Me_2 on the planar and the positive curvature structured electrode. With a longer pulse time, the contrast is reduced more with number of switch cycle when using the structured electrode. The contrast decrease is more noticeable when using the planar electrode. By switching to an ionic liquid (1-Butyl-3-methylimidazolium tetrafluoroborate, BMIM BF4) the contrast could be retained for over 10 million switches using short pulses (Figure 4c **Paper I)**. This can be attributed to fewer side reactions taking place, which could produce species that degrade the polymer.

4.3 Tungsten oxide

Utilizing the same method based on Lambert-Beer formalism to find the best thickness which generates the highest contrast was not possible for tungsten oxide. The real part of the refractive index is about 2.2 [68] and will generate a Fresnel reflection at the film's boundary and electrolyte. This leads to interference in the thin film when it is ~100 nm or more in thickness, which strongly influences the reflectivity spectrum. Therefore, complete Fresnel modeling was required to simulate the contrast against the thickness.

Since the tungsten oxide also created thin-film interference with the metasurface the modeling had to include all thin films (Figure 3D **Paper II**). The contrast is around 60% for all samples red, green, and blue of WO_3 on the metastructures (Figure 4B **Paper II**). The switching time is around 1 s to 10 s depending on the direction (Figure 5B **Paper II**). The bistability is nearly perfect, only a slight increase in intensity has emerged after 10'000s (Figure 6B **Paper II**).

5 Conclusion

Using abundant materials such as copper and aluminum to create colored metastructures was possible which opens up for a cheaper alternative than using the precious metals, silver, and gold. Good optical contrast was reached utilizing screen-printed PEDOT:PSS as electrochromic material. By using an aluminum mirror instead of a silver mirror as the back reflector for the colored metasurfaces it was possible to electropolymerize conjugated polymers directly on top of the surfaces in an organic solvent.

The method which gave the best polymer uniformity was using cyclic voltammetry with the organic solvent propylene carbonate. Three polymers were electropolymerized on a thin gold film and the optical contrast was compared. It was found that the polymer followed Lambert-Beer formalism which makes it possible to quickly determine the maximum contrast by measuring the optical extinction of the colored and the bleached state and using a formula that uses a ratio of the optical extinctions.

One polymer was electropolymerized on the colored pixels and compared with a sputtered inorganic electrochromic material, tungsten oxide. The optical contrast of the inorganic option was slightly higher than for the organic conjugated polymer. However, the switching speed was faster for the organic option than for the inorganic.

By altering the electrode structure or reducing the distance between the working and counter electrode, it was found that the switching time could be decreased until it reached video speed together with retaining the high optical contrast. The short pulse duration also made it possible to increase the lifetime to up to 10 million switches.

6 Future Outlook

The results presented in this thesis are from experiments done in a three-electrode setup. To further take a step towards making a reflective display, the electrochromic material will have to be pixelated in an active or passive matrix configuration. To be able to do this implementation the three-electrode setup needs to be reduced to a two-electrode setup and later made into an electrochromic device.

A passive matrix configuration is currently developed to realize a pixelated display. This uses perpendicular stripes of electrodes with the electrochromic material sandwiched in between. To do this the three-electrode setup needs to be eliminated and substituted with a two-electrode setup, which later will be transformed into an electrochromic device.

To make an electrochromic device a counter electrode, usually ITO, is implemented with an ion-storage layer coated on it. If using bare ITO as a counter electrode the voltage across the device will have to be increased to get the full contrast. This is attributed to ITOs inefficient ion-storage capacity at lower voltages. To lower the voltages of the device a counter material is incorporated on the counter electrode. This material is used to increase the ion-storage at the similar voltages of the main electrochromic material on the working electrode [69]. However, to make a passive matrix functional it is a requirement that the electro-optical function of the individual device is nonlinear and possesses hysteresis.

The electrochromic polymers do not possess any hysteresis and there is a one-to-one correspondence between applied potential and absorbance. By choosing the counter electrode wisely you can introduce this hysteresis and the device can be used in a passive matrix [70]. This will further be investigated.

An active-matrix configuration will also be constructed where conjugated polymers will be directly synthesized on a commercial thin-film transistor (TFT) -array. More structures will also be produced on the TFT-array such as the metasurfaces.

7 Acknowledgments

I would like to thank Swedish Foundation for Strategic Research (SSF) for the funding. I would like to thank my supervisor, Andreas Dahlin and my examiner, Christian Müller, for good discussions. I would like to thank my former colleagues, Philip Holgersson and Felix Karlsson, at RDOT. I would also like to thank Peter Andersson Ersman for all help regarding electrochromism and displays.

I would like to thank all my colleagues in the Dahlin group, especially Marika. And I would like to thank my family for support.

Göteborg, November, 2021

8 Bibliography

[1] *Handbook of Visual Display Technology*. Springer-Verlag Berlin Heidelberg, 2012.

[2] Y. Lu, B. Tang, G. Yang, Y. Guo, L. Liu, and A. Henzen, "Progress in Advanced Properties of Electrowetting Displays," *Micromachines,* vol. 12, no. 2, p. 206, 2021, doi: 10.3390/mi12020206.

[3] R. A. Hayes and B. J. Feenstra, "Video-speed electronic paper based on electrowetting," *Nature,* vol. 425, no. 6956, pp. 383-385, 2003, doi: 10.1038/nature01988.

[4] P. F. Bai *et al.*, "REVIEW OF PAPER-LIKE DISPLAY TECHNOLOGIES (Invited Review)," *Progress In Electromagnetics Research,* vol. 147, pp. 95-116, 2014, doi: 10.2528/pier13120405.

[5] M. Gugole, O. Olsson, S. Rossi, M. P. Jonsson, and A. Dahlin, "Electrochromic Inorganic Nanostructures with High Chromaticity and Superior Brightness," *Nano Letters,* vol. 21, no. 10, pp. 4343–4350, 2021, doi: 10.1021/acs.nanolett.1c00904.

[6] M. Omodani, "10.1: Invited Paper: What is Electronic Paper? The Expectations," *SID Symposium Digest of Technical Papers,* vol. 35, no. 1, p. 128, 2004, doi: 10.1889/1.1825751.

[7] K. Xiong, D. Tordera, M. P. Jonsson, and A. B. Dahlin, "Active control of plasmonic colors: emerging display technologies," *Reports on Progress in Physics,* vol. 82, no. 2, p. 024501, 2019, doi: 10.1088/1361-6633/aaf844.

[8] S. Daqiqeh Rezaei *et al.*, "Nanophotonic Structural Colors," *ACS Photonics,* vol. 8, no. 1, pp. 18–33, 2020, doi: 10.1021/acsphotonics.0c00947.

[9] D. Franklin, R. Frank, S.-T. Wu, and D. Chanda, "Actively addressed single pixel full-colour plasmonic display," *Nature Communications,* vol. 8, p. 15209, 2017, doi: 10.1038/ncomms15209.

[10] K. Xiong *et al.*, "Plasmonic Metasurfaces with Conjugated Polymers for Flexible Electronic Paper in Color," *Advanced Materials,* vol. 28, no. 45, pp. 9956-9960, 2016, doi: 10.1002/adma.201603358.

[11] S. Kinoshita, S. Yoshioka, and J. Miyazaki, "Physics of structural colors," *Reports on Progress in Physics,* vol. 71, no. 7, p. 076401, 2008.

[12] A. Kristensen *et al.*, "Plasmonic colour generation," *Nature Reviews Materials,* vol. 2, no. 1, p. 16088, 2017, doi: 10.1038/natrevmats.2016.88.

[13] S. A. Maier, *Plasmonics: fundamentals and applications*. Springer Science & Business Media, 2007.

[14] T. Sannomiya, O. Scholder, K. Jefimovs, C. Hafner, and A. B. Dahlin, "Investigation of Plasmon Resonances in Metal Films with Nanohole Arrays for Biosensing Applications," *Small,* vol. 7, no. 12, pp. 1653-1663, 2011, doi: 10.1002/smll.201002228.

[15] J. Junesch, T. Sannomiya, and A. B. Dahlin, "Optical Properties of Nanohole Arrays in Metal–Dielectric Double Films Prepared by Mask-on-Metal Colloidal Lithography," *ACS Nano,* vol. 6, no. 11, pp. 10405-10415, 2012, doi: 10.1021/nn304662e.

[16] A. B. Dahlin, M. Mapar, K. Xiong, F. Mazzotta, F. Höök, and T. Sannomiya, "Plasmonic Nanopores in Metal-Insulator-Metal Films," *Advanced Optical Materials,* vol. 2, no. 6, pp. 556-564, 2014, doi: 10.1002/adom.201300510.

[17] K. Xiong *et al.*, "Switchable Plasmonic Metasurfaces with High Chromaticity Containing Only Abundant Metals," *Nano Letters,* vol. 17, no. 11, pp. 7033-7039, 2017, doi: 10.1021/acs.nanolett.7b03665.

[18] A. J. Bard and L. R. Faulkner, *Electrochemical Methods: Fundamentals and Applications*. John Wiley & Sons, Incorporated, 2001.

[19] J. H. Brown, "Development and Use of a Cyclic Voltammetry Simulator To Introduce Undergraduate Students to Electrochemical Simulations," *Journal of Chemical Education,* vol. 92, no. 9, pp. 1490-1496, 2015, doi: 10.1021/acs.jchemed.5b00225.

[20] R. G. Compton, E. Kätelhön, K. R. Ward, and E. Laborda, *Understanding voltammetry: simulation of electrode processes*. World Scientific, 2014.

[21] A. J. Coffman, J. Lu, and J. E. Subotnik, "A grid-free approach for simulating sweep and cyclic voltammetry," *The Journal of Chemical Physics,* vol. 154, no. 16, p. 161101, 2021, doi: 10.1063/5.0044156.

[22] R. J. Mortimer, "Electrochromic Materials," *Annual Review of Materials Research,* vol. 41, no. 1, pp. 241-268, 2011, doi: 10.1146/annurev-matsci-062910-100344.

[23] R. J. Mortimer, "Organic electrochromic materials," *Electrochimica Acta,* vol. 44, no. 18, pp. 2971-2981, 1999, doi: 10.1016/s0013-4686(99)00046-8.

[24] A. Köhler and H. Bässler, *Electronic processes in organic semiconductors: An introduction*. John Wiley & Sons, 2015.

[25] M. Heydari Gharahcheshmeh and K. K. Gleason, "Texture and nanostructural engineering of conjugated conducting and semiconducting polymers," *Materials Today Advances,* vol. 8, p. 100086, 2020, doi: 10.1016/j.mtadv.2020.100086.

[26] D. N. Batchelder, "Colour and chromism of conjugated polymers," *Contemporary Physics,* vol. 29, no. 1, pp. 3-31, 1988, doi: 10.1080/00107518808213749.

[27] O. Bubnova and X. Crispin, "Towards polymer-based organic thermoelectric generators," *Energy & Environmental Science,* vol. 5, no. 11, p. 9345, 2012, doi: 10.1039/c2ee22777k.

[28] A. O. Patil, A. J. Heeger, and F. Wudl, "Optical properties of conducting polymers," *Chemical Reviews,* vol. 88, no. 1, pp. 183-200, 1988, doi: 10.1021/cr00083a009.

[29] J. L. Bredas and G. B. Street, "Polarons, bipolarons, and solitons in conducting polymers," *Accounts of Chemical Research,* vol. 18, no. 10, pp. 309-315, 1985, doi: 10.1021/ar00118a005.

[30] A. Moliton and R. C. Hiorns, "Review of electronic and optical properties of semiconductingπ-conjugated polymers: applications in optoelectronics," *Polymer International,* vol. 53, no. 10, pp. 1397-1412, 2004, doi: 10.1002/pi.1587.

[31] P. Camurlu, "Polypyrrole derivatives for electrochromic applications," *RSC Advances,* vol. 4, no. 99, pp. 55832-55845, 2014, doi: 10.1039/c4ra11827h.

[32] I. Zozoulenko, A. Singh, S. K. Singh, V. Gueskine, X. Crispin, and M. Berggren, "Polarons, Bipolarons, And Absorption Spectroscopy of PEDOT," *ACS Applied Polymer Materials,* vol. 1, no. 1, pp. 83-94, 2019, doi: 10.1021/acsapm.8b00061.

[33] P. M. Beaujuge and J. R. Reynolds, "Color Control in π-Conjugated Organic Polymers for Use in Electrochromic Devices," *Chemical Reviews,* vol. 110, no. 1, pp. 268-320, 2010, doi: 10.1021/cr900129a.

[34] D. M. Welsh, A. Kumar, E. W. Meijer, and J. R. Reynolds, "Enhanced Contrast Ratios and Rapid Switching in Electrochromics Based on Poly(3,4-propylenedioxythiophene)

Derivatives," *Advanced Materials,* vol. 11, no. 16, pp. 1379-1382, 1999, doi: 10.1002/(sici)1521-4095(199911)11:16<1379::Aid-adma1379>3.0.Co;2-q.

[35] A. Kumar, D. M. Welsh, M. C. Morvant, F. Piroux, K. A. Abboud, and J. R. Reynolds, "Conducting Poly(3,4-alkylenedioxythiophene) Derivatives as Fast Electrochromics with High-Contrast Ratios," *Chemistry of Materials,* vol. 10, no. 3, pp. 896-902, 1998, doi: 10.1021/cm9706614.

[36] I. Schwendeman *et al.*, "Enhanced Contrast Dual Polymer Electrochromic Devices," *Chemistry of Materials,* vol. 14, no. 7, pp. 3118-3122, 2002, doi: 10.1021/cm020050y.

[37] J. Hwang, D. B. Tanner, I. Schwendeman, and J. R. Reynolds, "Optical properties of nondegenerate ground-state polymers: Three dioxythiophene-based conjugated polymers," *Physical Review B,* vol. 67, no. 11, 2003, doi: 10.1103/physrevb.67.115205.

[38] X. Li, K. Perera, J. He, A. Gumyusenge, and J. Mei, "Solution-processable electrochromic materials and devices: roadblocks and strategies towards large-scale applications," *Journal of Materials Chemistry C,* vol. 7, no. 41, pp. 12761-12789, 2019, doi: 10.1039/c9tc02861g.

[39] B. Winther-Jensen, J. Chen, K. West, and G. Wallace, "Vapor Phase Polymerization of Pyrrole and Thiophene Using Iron(III) Sulfonates as Oxidizing Agents," *Macromolecules,* vol. 37, no. 16, pp. 5930-5935, 2004, doi: 10.1021/ma049365k.

[40] P. Andersson, R. Forchheimer, P. Tehrani, and M. Berggren, "Printable All-Organic Electrochromic Active-Matrix Displays," *Advanced Functional Materials,* vol. 17, no. 16, pp. 3074-3082, 2007, doi: 10.1002/adfm.200601241.

[41] R. Brooke *et al.*, "Infrared electrochromic conducting polymer devices," *Journal of Materials Chemistry C,* vol. 5, no. 23, pp. 5824-5830, 2017, doi: 10.1039/c7tc00257b.

[42] G. Sabouraud, S. Sadki, and N. Brodie, "The mechanisms of pyrrole electropolymerization," *Chemical Society Reviews,* vol. 29, no. 5, pp. 283-293, 2000, doi: 10.1039/a807124a.

[43] E. Smela, "Microfabrication of PPy microactuators and other conjugated polymer devices," *Journal of micromechanics and microengineering,* vol. 9, no. 1, p. 1, 1999.

[44] J. R. Heinze, B. A. Frontana-Uribe, and S. Ludwigs, "Electrochemistry of Conducting Polymers—Persistent Models and New Concepts†," *Chemical Reviews,* vol. 110, no. 8, pp. 4724-4771, 2010, doi: 10.1021/cr900226k.

[45] B. J. West, T. F. Otero, B. Shapiro, and E. Smela, "Chronoamperometric Study of Conformational Relaxation in PPy(DBS)," *The Journal of Physical Chemistry B,* vol. 113, no. 5, pp. 1277-1293, 2009, doi: 10.1021/jp8058245.

[46] T. F. Otero, "Electroactive macromolecular motors as model materials of ectotherm muscles," *RSC Advances,* vol. 11, no. 35, pp. 21489-21506, 2021, doi: 10.1039/d1ra02573b.

[47] S. W. Feldberg, "Reinterpretation of polypyrrole electrochemistry. Consideration of capacitive currents in redox switching of conducting polymers," *Journal of the American Chemical Society,* vol. 106, no. 17, pp. 4671-4674, 1984, doi: 10.1021/ja00329a004.

[48] T. F. Otero, H.-J. Grande, and J. Rodríguez, "Reinterpretation of Polypyrrole Electrochemistry after Consideration of Conformational Relaxation Processes," *The Journal of Physical Chemistry B,* vol. 101, no. 19, pp. 3688-3697, 1997, doi: 10.1021/jp9630277.

[49] T. F. Otero and J. Padilla, "Anodic shrinking and compaction of polypyrrole blend: electrochemical reduction under conformational relaxation kinetic control," *Journal of Electroanalytical Chemistry,* vol. 561, pp. 167-171, 2004, doi: 10.1016/j.jelechem.2003.08.001.

[50] X. Wang, B. Shapiro, and E. Smela, "Development of a Model for Charge Transport in Conjugated Polymers," *The Journal of Physical Chemistry C,* vol. 113, no. 1, pp. 382-401, 2009, doi: 10.1021/jp802941m.

[51] A. V. Volkov *et al.*, "Understanding the Capacitance of PEDOT:PSS," *Advanced Functional Materials,* vol. 27, no. 28, p. 1700329, 2017, doi: 10.1002/adfm.201700329.

[52] W. Lu, "Use of Ionic Liquids for pi -Conjugated Polymer Electrochemical Devices," *Science,* vol. 297, no. 5583, pp. 983-987, 2002, doi: 10.1126/science.1072651.

[53] X. Wang *et al.*, "Mechanical breathing in organic electrochromics," *Nature Communications,* vol. 11, no. 1, 2020, doi: 10.1038/s41467-019-14047-8.

[54] P. Tehrani, A. Kanciurzewska, X. Crispin, N. Robinson, M. Fahlman, and M. Berggren, "The effect of pH on the electrochemical over-oxidation in PEDOT:PSS films," *Solid State Ionics,* vol. 177, no. 39-40, pp. 3521-3527, 2007, doi: 10.1016/j.ssi.2006.10.008.

[55] H. Tang, L. Zhu, Y. Harima, and K. Yamashita, "Chronocoulometric determination of doping levels of polythiophenes: influences of overoxidation and capacitive processes," *Synthetic Metals,* vol. 110, no. 2, pp. 105-113, 2000, doi: 10.1016/s0379-6779(99)00269-6.

[56] J. Padilla, V. Seshadri, G. Sotzing, and T. Otero, "Maximum contrast from an electrochromic material," *Electrochemistry Communications,* vol. 9, no. 8, pp. 1931-1935, 2007, doi: 10.1016/j.elecom.2007.05.004.

[57] K. Yuan, Yan, Hui-min, Jin, Shang-zhong, "The design of color spectrophotometer based on diffuse illumination and compatible SCE/SCI geometric condition," presented at the Proc. SPIE 9046, 2013 International Conference on Optical Instruments and Technology: Optoelectronic Measurement Technology and Systems, 2013. [Online]. Available: https://dx.doi.org/10.1117/12.2036508.full.

[58] T. Smith and J. Guild, "The C.I.E. colorimetric standards and their use," *Transactions of the Optical Society,* vol. 33, no. 3, pp. 73-134, 1931, doi: 10.1088/1475-4878/33/3/301.

[59] C. Oleari, *Standard Colorimetry : Definitions, Algorithms and Software*. New York, UNITED KINGDOM: John Wiley & Sons, Incorporated, 2016.

[60] P.-H. Aubert, A. A. Argun, A. Cirpan, D. B. Tanner, and J. R. Reynolds, "Microporous Patterned Electrodes for Color-Matched Electrochromic Polymer Displays," *Chemistry of Materials,* vol. 16, no. 12, pp. 2386-2393, 2004, doi: 10.1021/cm049951s.

[61] A. A. Argun, M. Berard, P. H. Aubert, and J. R. Reynolds, "Back-Side Electrical Contacts for Patterned Electrochromic Devices on Porous Substrates," *Advanced Materials,* vol. 17, no. 4, pp. 422-426, 2005, doi: 10.1002/adma.200401353.

[62] A. A. Argun and J. R. Reynolds, "Line patterning for flexible and laterally configured electrochromic devices," *Journal of Materials Chemistry,* vol. 15, no. 18, p. 1793, 2005, doi: 10.1039/b417607c.

[63] T. F. Otero and E. De Larreta, "Electrochemical control of the morphology, adherence, appearance and growth of polypyrrole films," *Synthetic Metals,* vol. 26, no. 1, pp. 79-88, 1988/10/01/ 1988, doi: https://doi.org/10.1016/0379-6779(88)90337-2.

[64] P. Schottland *et al.*, "Poly(3,4-alkylenedioxypyrrole)s: Highly Stable Electronically Conducting and Electrochromic Polymers," *Macromolecules,* vol. 33, no. 19, pp. 7051-7061, 2000, doi: 10.1021/ma000490f.

[65] T. Johansson, N.-K. Persson, and O. InganäS, "Moving Redox Fronts in Conjugated Polymers Studies from Lateral Electrochemistry in Polythiophenes," *Journal of The Electrochemical Society,* vol. 151, no. 4, p. E119, 2004, doi: 10.1149/1.1649749.

[66] V. Syritski, A. Öpik, and O. Forsén, "Ion transport investigations of polypyrroles doped with different anions by EQCM and CER techniques," *Electrochimica Acta,* vol. 48, no. 10, pp. 1409-1417, 2003, doi: 10.1016/s0013-4686(03)00018-5.

[67] J.-H. Huang, C.-Y. Hsu, C.-W. Hu, C.-W. Chu, and K.-C. Ho, "The Influence of Charge Trapping on the Electrochromic Performance of Poly(3,4-alkylenedioxythiophene) Derivatives," *ACS Applied Materials & Interfaces,* vol. 2, no. 2, pp. 351-359, 2010, doi: 10.1021/am900752m.

[68] C. A. Triana, C. G. Granqvist, and G. A. Niklasson, "Electrochromism and small-polaron hopping in oxygen deficient and lithium intercalated amorphous tungsten oxide films," *Journal of Applied Physics,* vol. 118, no. 2, p. 024901, 2015, doi: 10.1063/1.4926488.

[69] D. Eric Shen, A. M. Österholm, and J. R. Reynolds, "Out of sight but not out of mind: the role of counter electrodes in polymer-based solid-state electrochromic devices," *Journal of Materials Chemistry C,* vol. 3, no. 37, pp. 9715-9725, 2015, doi: 10.1039/c5tc01964h.

[70] P. Andersson Ersman, J. Kawahara, and M. Berggren, "Printed passive matrix addressed electrochromic displays," *Organic Electronics,* vol. 14, no. 12, pp. 3371-3378, 2013, doi: 10.1016/j.orgel.2013.10.008.